Lawrence Berkeley Laboratory
UNIVERSITY OF CALIFORNIA

Materials & Molecular Research Division

THE FIRST GENERATION OF BUBBLES AT GAS EVOLVING ELECTRODES

P. Cettou and C.W. Tobias

December 1981

Prepared for the U.S. Department of Energy under Contract DE-AC03-76SF00098

DISCLAIMER

LBL-13632

THE FIRST GENERATION OF BUBBLES AT GAS EVOLVING ELECTRODES

P. Cettou, with C. W. Tobias

Lawrence Berkeley Laboratory
University of California
Berkeley, California

December 5, 1981

This work was supported by the Assistant Secretary for Conservation and Solar Energy, Office of Advanced Conservation Technology, Electrochemical Systems Research Division of U. S. Department of Energy under Contract Number DE-AC03-76SF00098.

THE FIRST GENERATION OF BUBBLE AT GAS EVOLVING ELECTRODES

Contents

THE FIRST GENERATION OF BUBBLES AT GAS EVOLVING ELECTRODES

P. Cettou, with C. W. Tobias

Lawrence Berkeley Laboratory
University of California
Berkeley, California 94720

Abstract

We have observed the growth of the first generation of bubbles at gas-evolving electrodes by high speed motion picture and measured the increase of the electrical resistance during this period. The resistance of the bubble layer constitutes a significant part of the overall cell resistance. To reduce this resistance, either the electrode coverage or the bubble layer thickness can be lowered. Our studies show that strong coalescence, which occurs most readily in sulfuric acid, promotes both of these desired effects.

Relations & Nomenclature

$R = E/I = 1/kA$

$k = k(T)$

R_o = electrical resistance without bubbles [ohm]

R_t = electrical resistance with bubbles

$\Delta R = R_t - R_o$

C_o = cell constant without bubbles [cm^{-1}]

C_t = cell constant with bubbles

$R^* = dR/R_o = R_t - R_o$ /R# = reduced resistance

R# = average value of R_o

l = electrode separation

d = bubble diameter = layer thickness

$d^* = d/l$ = reduced layer thickness

k_o = conductivity of the electrolyte [ohm^{-1} cm^{-1}]

k_b = conductivity of the bubble layer

$k^* = kb/ko$ = reduced conductivity

$R_b = d/k_bA$

$R_o = 1/k_oA$

$R_t = d/k_bA + 1/(1 - d/l)$

$R_t = R_b + R_o(1 - d/l)/k_oA$

$k^* = d^* /(R^* + d^*)$

$G = jV/zF$, specific gas production rate, $[cm^3/cm^2\text{-}s]$

or $[cm^3/cm^2\text{-}min]$

$j = I/A$ = current density, $[A/cm^2]$

A = electrode area (w = working, c = counter, r = reference), $[cm^2]$

V = volume, $[cm^3]$

P = pressure, [atm]

T = temperature, $[^oC]$

n = number density, $[bubbles/cm^2]$

no = nucleation density, $[nuclei/cm^2]$

d = diameter, [cm]

v = velocity, [cm/s]

Δt_1 = initiation time, [s]

Δt_2 = residence time of bubbles on the surface, [s]

f = electrode coverage = $n\pi d^2/4$

e = void fraction = $n\pi d^2/6$

1. Introduction

Industrial electrolytic processes with gas evolution account for more than two percent of the total US energy consumption. Such processes include the production of aluminium, chlorine and hydrogen as well as the preparation of chlorates, bromates and certain organic compounds.

Despite its prevalence, gas evolution has received only little attention from scientific investigators. In view of the recent energy cost increase, a closer study of this phenomenon is needed in order to make these processes more efficient.

One of the key problems associated with the presence of gas bubbles in an electrolytic cell is the rise of the overall cell voltage, which can occur in two ways:

-- The gas hold-up in the interelectrode gap, referred to as the bubbles in the bulk, reduces the effective electrical conductivity of the bulk electrolyte;

-- The bubbles in the vicinity of the electrode, referred to as the bubble layer, shield the electrode surface and reduce its accessibility; the current is forced to flow through a smaller cross-section of electrolyte and this results in a higher ohmic drop.

Practical improvements of cell and electrode design have largely eliminated the resistance caused by bubbles in the bulk. The bubble layer, however, remains a problem and its characteristics are not well known. The literature indicates that the voltage drop across this layer

can be hundreds of millivolts. Thus, the properties and the behavior of this layer deserve attention.

In steady-state gas evolution, bubbles are present both in the bulk electrolyte and at the electrode surface. However, just after the current is turned on, only the bubble layer is present. Thus, during this initial period, the events occurring at the electrode surface are easily observed. In addition, the contribution of the bubble layer to the total cell resistance can be measured at this time. For these reasons, we chose to study the first generation of bubbles at the electrode.

In the research described in this report, the evolution of hydrogen and oxygen was observed on three different electrode materials (gold, nickel and stainless steel) and with three different electrolytes (sodium hydroxide, sodium sulfate and sulfuric acid). The influence of current density was also investigated.

The events associated with gas evolution--nucleation, growth by diffusion and by coalescence, and departure from the electrode--occur rapidly and on a small scale. Some observations of this incipient period were made by Putt [1], in 1975, using still photography. However, to reveal more details of these events, we used high speed cinematography with a microscope.

The dependence of electrical resistance upon electrode coverage was determined experimentally by a conventional interrupted current technique. The results are compared with predictions from established theoretical models.

2. Literature Review

The study of electrolytically generated gas bubbles has been conducted for a long time in our laboratory. As early as 1958, Tobias [2] published a paper, recognized today as classical, describing and discussing the effects of gas evolution on current distribution and ohmic resistance in electrolyzers.

In 1967, Cheh [3] conducted a theoretical treatment of various phenomena associated with gas evolution; bubble nucleation, growth and separation, and also growth rates of rising bubbles were analysed. The effects of interaction between bubbles were not included in this treatment.

Bon [4] measured the supersaturation of dissolved gas at a gas-evolving electrode. For this purpose, he used an original technique (micro-measuring electrodes positioned inside the diffusion layer). At $j = 100\ mA/cm^2$, he typically found the hydrogen supersaturation at the surface to be 100 atm.

R. Putt [1] photographed bubbles from the front of nickel electrodes. To document the incipient bubble growth period, he evolved gas for given short periods of time before triggering his still camera. From the analysis of the picture sequences, he concluded that bubbles grow not only by diffusion of dissolved gas, but also by coalescence of existing bubbles. He proposed that the bubble departure at industrial gas evolution rates is governed by the dynamics of the bubble interactions.

P. Sides [5] used high-speed cinematography to observe oxygen evolution at steady state from the backside of a transparent electrode. The movies showed, among other things, that coalescence is a relatively important mode of bubble growth and affects the hydrodynamics close to the electrode. The author solved Laplace's equation to obtain the potential field and current distribution around an insulating sphere on a planar electrode [6]. The solution allowed him to calculate the resistance increase caused by a sparse array of bubbles on an electrode. For a dense array of bubbles, the resistance increase was determined from a physical model, which showed that the electrical resistance sharply increased as close packing was approached.

W. C. Hui [7] studied how the incremental resistance caused by gas bubbles is decreased by forced flow and by various surface finishes of the electrode. Optical observation and electrical measurement were carried out simultaneously in a flow channel.

For more complete background, the reader is referred to literature reviews by each of the above authors, which summarize the status of the field quite comprehensively. The following two contributions could be added.

In Milan, research on electrolytic gas evolution, initiated by Prof. Piontelli, has been carried out for some 15 years. Some of the results are presented in three long articles (unfortunately in italian) [8]. Extensive studies on the morphological aspects of gas evolution for a wide range of experimental conditions were made using high speed cinematography. In particular, the factors influencing the nucleation, growth, departure and coalescence were analysed. The conditions for the

occurence of the anode (or cathode) effect were also examined, and, more recently, a general explanation based on the conditions of hydrodynamic instability was published [9].

At the occasion of an international colloquium for interdisciplinary exchange in the science of drops and particles, a very general and interesting summary on the subject was given by L.E. Scriven [10]. Turning to more current work, the Second International Colloquium on Drops and Bubbles was just held in November 1981; a proceeding of this meeting is expected for the beginning of next year.

Some recent papers have been published by the few groups working on electrolytic gas evolution.

In Japan, F. Hine et al. have been working for a long time on electrolyzers with parallel vertical electrodes. Their most recent communications are described below.

In "the bubble effects on the solution IR drop under free and forced convection" [11]. The authors show the validity of the Bruggeman's equation for relating resistivity to void fraction. Tobias's equation, which expresses the local current density is also verified. The performance of the cell increases sharply when the electrolyte is recirculated. The anode-to-cathode gap is a major component of the terminal cell voltage and was found to be optimal at 5 to 7 mm, depending on operating conditions.

Another way of minimizing unwanted bubble effects was also investigated: the use of perforated electrodes [12]. Although the reduction of the surface area of such electrodes is an important disadvantage, the

results showed that with 5-15 percent perforations the solution IR drop is minimized.

Lately, Helmut Vogt produced three papers dealing with gas evolving electrodes. The first one [13] investigates heat transfer on such electrodes. As the existing Zuber-Magrini method for prediction of heat transfer is difficult to apply, the author proposes an alternative method: taking advantage of the analogy, existing theoretical equations for mass transfer are applied to heat transfer.

The second paper [14] treats the supersaturation of electrogenerated products in the concentration boundary layer of gas evolving electrodes. A comparison of data obtained by different methods and a discussion of the concentration distribution in the boundary layer leads to a distinction between a supersaturation threshold for nucleation and a different one for bubble growth.

The third paper [15] proposes a hydrodynamic model for IR drop in vertical electrolyzers. This model differs from Tobias's equation in the assumption of a separation of the ohmic resistance into two parts: one due to a stagnant boundary layer at the electrode(s) and the other due to the flowing bulk in the center region.

Other recent work on parallel vertical electrodes systems is presented by R. Alkyre [16] and Hamzah and Kuhn [17]. The first one was an investigation of the effect of hydrogen evolution on current distribution during electrodeposition. Two kinds of mass transfer effects occur simultaneously: stirring caused by detaching bubbles and stirring caused by rising bubbles.

The second paper examined the roles of the surface texture and of anode-cathode size ratio on mass transfer. The effect of cathode roughness can be explained in terms of bubble obscuration, much less prominent on smooth surfaces than on a rough ones. The bubble obscuration on rough surfaces outweighs the benefit of increased surface area.

To remove gas bubbles from the interelectrode gap, Jorne [18] proposed a gas-diverting electrode made of unflattened expanded metal sheets. A significant drop of the cell potential as well as an increase in current efficiency are reported. Moreover, such an electrode eliminates the restriction of the cell's height and of the minimal gap.

Since most of the area of expanded metal electrodes consists of inclined planes, Kreysa and Kuelps [19] found that slightly up-facing oriented electrodes (15^{o}) have a gas layer of an optimum state in terms of minimizing IR drop.

In his study of the mass transfer at gas-evolving electrodes, Janssen [20] concluded that the hydrodynamic model [21] is valid when no coalescence of gas bubbles occurs and that the penetration model [22] can explain the mass transfer when coalescence occurs frequently. Later, he proposed another model to describe mass transfer for the latter case, the coalescence model [23]. To check this model, both the thickness of Nernst diffusion layer and the bubble behaviour were determined for oxygen evolution on a nickel transparent electrode in potassium hydroxide.

Iwakura et al. [24] present the anodic polarization characteristics for the evolution of oxygen and chlorine on foreign-metal-doped SnO_2 film electrodes.

Denton et al. [25] studied the electrode kinetics and electrochemical characteristics of the oxygen evolution on RuO_2-TiO_2 electrodes.

A review of an interesting method for counting bubbles is presented by Medwin [26]: counting bubbles acoustically. The large scattering cross-section at resonance combined with the fact that the resonance frequency is inversely proportional to the bubble radius make a variable-frequency backscatter experiment a feasible technique for obtaining the number density of bubbles as a function of radius, providing that much larger scatterers are absent. The limitations arise from interactions among the bubbles, which perturb the signal.

3. Observations

3.1. Goal

The purpose of this present study is to extend our understanding of the physical events occuring during the evolution of gases from electrode surfaces. We want to observe the bubble layer behavior under different experimental conditions such as:

- the nature of the gas evolved
- the nature of electrodes and electrolytes
- the current density.

These observations must be made during the incipient evolution of bubbles, i.e., the few seconds following the onset of the current. In this manner, the view of the electrode surface is not obstructed by bubbles rising in the electrolyte bulk.

3.2. Experimental

3.2.1. Observation Cell, Electrodes and Electrolytes

Frontal observation of a metallic electrode is made through an optical microscope by a high speed camera. The figure 3.1. shows the cell assembly. The cell block is transparent, made of Lucite. It has vertical electrodes and stagnant electrolyte, each easily interchangeable. The distance between the cell wall and the working electrode is small to allow for the short focal length of the microscope objective. The observed portion of the electrode surface is its center.

Three variations of this cell were used: PSA, PSB and PCA (cf. figure 3.1.).

Three different working electrodes were used:

1. plain stainless steel 304
2. plain nickel 200
3. electrodeposited gold on stainless steel (50 microns, nickel flash).

These electrodes are given the same surface preparation:

- polishing with 1-micron diamond paste in kerosene lubricant
- rinsing with soap, water and alcohol
- polishing with 0.05-micron aluminium oxide in water
- rinsing and ultrasonic treatment in water
- alternate anodic and cathodic polarization
- the last prepolarization is of the same polarity as the one we investigate, for 15 minutes with 20 mA/cm^2.

Three aqueous electrolytes are used. Their physical properties (viscosity and conductivity) are presented in figure 3.2.

Electrolyte	Concentration [M]	Conductivity [mho/cm]
Sodium hydroxide	1	165
Sodium sulfate	2	120
Sulfuric acid	0.4	165

Hydrogen and oxygen evolution are observed in that cell.

3.2.2. Cinematographic Technique [27, 28]

The electrode is filmed through a microscope with a high speed camera. The observed area of the surface is approximately 4 mm by 3 mm. The speed of the rotating-prism camera can be varied from 20 to 11,000 frames per second (fps); the speed can be verified by marks on the film, made by a built-in timing light generator. This camera uses 16 mm film, up to 400 feet long. We use a reversal black-and-white film, delivered in rolls of 100 feet. Approximately one third of the roll is used before the chosen speed of 2000 fps is reached. There are 40 frames per foot, and the projection rate is generally 24 fps. With such conditions, the events are slowed down by a factor of 83. In other words, one second in real time is projected for 83 seconds.

Camera: HYCAM 41-0004

Film: KODAK Tri-X reversal 7278, 100 feet, 200 ASA
KODAK 4-X reversal 7277, 100 feet, 400 ASA

3.2.3. Experimental Set-Up

Figure 3.3. shows schematically the set-up of the observation experiment.

When the camera has accelerated to the desired speed, a constant current step is imposed. At this instant, a flash is triggered which marks on the film the start of the electrolysis. The camera has a built-in switch which actuates for a predeterminated length of the film. This switch is used to trigger the onset of the current and the photographic flash, when the film has reached the steady speed of 2000 fps.

3.3. Results

3.3.1. Sequence of Events

The figure 3.4. shows the sequence of events recorded on the film.

Immediately after the onset of the current, there is an initiation period, during which there are no bubbles on the electrode surface. During this period, the electrical current is used for:

- charging the electrical double layer at the interface electrode/solution
- increasing the dissolved gas concentration in the vicinity of the electrode.

When the supersaturation is high enough, the nucleation of gas bubbles takes place.

The period following nucleation, refered to as the incipient growth period, sees bubble growth on the surface, by diffusion and coalescence. All the bubbles have approximately the same size and reach their detachement size at roughly the same time. During the transition period, the detached bubbles rise to the electrolyte surface and convey fluid along with them, setting up a hydrodynamic pattern. From this moment on, the timing of the events becomes random, because of the interaction between bubbles layer and rising bubbles. We can sometimes see scavenging coalescence: large bubbles sliding along the electrode surface absorbing the small ones. The steady state is attained when the volumetric flow of gas out of the cell is equal to the volumetric flow of produced gas at the electrode.

Until detachement occurs, the successive events are quite distinct. Therefore, we can define the following characteristics:

- initiation time Δt_1
- incipient growth time Δt_2
- nucleation density no
- average bubble diameter at detachement d_1.

Also, during the growth period, estimates of electrode coverage and coalescence frequency can be made.

The average bubble diameter in the bulk after 1 second of electrolysis, d_2, is also measured.

The table below is a list of all the movies we have made.

A. Influence of the prepolarization (presented at seminar 11.11.80)

This movie shows the special importance of the anodic prepolarization for oxygen evolution. When this prepolarization is made, a much higher nucleation density results.

Experimental conditions: 2000 fps
NaOH 0.2 M
PSA cell, Aw = 2.12 cm^2
I = 1.0 A $G(H_2) = 3.27\ cm^3/cm^2 min$
$G(O_2) = 1.64\ cm^3/cm^2 min$

Sequences		Real time [seconds]	Projection time [s] [seconds]
Hydrogen, cathodic prepolarization	(1)	1.2	100
Oxygen, new polished electrode	(2)	1.2	100
- the 3rd second	(3)	0.24	20
- the 5th second	(4)	0.24	20
- the 7th second	(5)	0.24	20
Oxygen, anodic prepolarization	(6)	1.2	100
Oxygen, anodic prepolarization	(7)	1.8	150

Please, look particularily at:

- on (1): the almost crystalline conformation of the bubble array
- on (2) to (5): the increase of the number density with time
- on (2) & (6) : the great influence of the prepolarization
- on (7): the scavenging coalescence; the rising bubbles leave a trail behind them.

B. Movies on Gold (2000 fps)

Number	Gas	Electrolyte	Cell	I[mA]	j[mA/cm^2]	G[cm^3/cm^{2}min]
12.16.80-1	O_2	NaOH	PSA	-450	-180	0.62
12.16.80-3	H_2	NaOH	PSA	+900	+360	2.5
12.16.80-4	O_2	H_2SO_4	PSA	-450	-180	0.62
12.16.80-5	H_2	H_2SO_4	PSA	+900	+360	2.5
12.16.80-6	O_2	Na_2SO_4	PSA	-450	-180	0.62
12.16.80-7	H_2	Na_2SO_4	PSA	+900	+360	2.5
12.18.80-1	H_2	NaOH	PSA	+450	+180	1.25
12.18.80-3	O_2	NaOH	PSA	-900	-360	1.25
12.18.80-4	H_2	H_2SO_4	PSA	+450	+180	1.25
12.18.80-5	O_2	H_2SO_4	PSA	-900	-360	1.25
12.18.80-6	H_2	Na_2SO_4	PSA	+450	+180	1.25
12.18.80-8	O_2	Na_2SO_4	PSA	-900	-360	1.25

C. Movies on nickel

01.16.81-1	H_2	NaOH	PSA	+450	+180	1.25
01.16.81-4	O_2	NaOH	PSA	-900	-360	1.25
01.16.81-5	H_2	Na_2SO_4	PSA	+450	+180	1.25
01.16.81-7	O_2	Na_2SO_4	PSA	-900	-360	1.25
01.16.81-8	H_2	H_2SO_4	PSA	+450	+180	1.25
01.16.81-9	O_2	H_2SO_4	PSA	-900	-360	1.25

01.21.81-1	H_2	Na_2SO_4	PSA	+200	+80	0.55
01.21.81-3	O_2	Na_2SO_4	PSA	-400	-160	0.55
01.30.81-1	H_2	H_2SO_4	PSA	+200	+80	0.55
01.30.81-3	O_2	H_2SO_4	PSA	-400	-160	0.55
02.03.81-1	H_2	NaOH	PSB	+84.5	+200	1.4
02.03.81-2	H_2	NaOH	PSB	+211.2	+500	3.5
02.03.81-3	H_2	NaOH	PSB	+422.5	+1000	7.0
02.03.81-4	H_2	NaOH	PSB	+845	+2000	14.0
08.17.81-1	H_2	NaOH	PSB	+76	+180	1.25
08.17.81-2	O_2	NaOH	PSB	-152	-360	1.25
08.17.81-3	H_2	H_2SO_4	PSB	+76	+180	1.25

D. Movies on Stainless Steel (2000 fps)

03.07.81-1	H_2	NaOH	PSB	+84.5	+200	1.4	
03.07.81-3	O_2	NaOH	PSB	-169	-400	1.4	
03.08.81-1	H_2	Na_2SO_4	PSB	+84.5	+200	1.4	
03.08.81-3	O_2	Na_2SO_4	PSB	-169	-400	1.4	
03.08.81-4	H_2	H_2SO_4	PSB	+84.5	+200	1.4	
03.08.81-6	O_2	H_2SO_4	PSB	-169	-400	1.4	
05.19.81-2	O_2	NaOH	PCA	-385	-500	1.75	
07.02.81-1	H_2	NaOH	PCA	+192	+250	1.75	1000 fps
07.02.81-2	O_2	NaOH	PCA	-385	-500	1.75	1000
07.13.81-1	H_2	NaOH	PCA	+192	+250	1.75	870
07.13.81-2	O_2	NaOH	PCA	-385	-500	1.75	870
07.29.81-1	H_2	NaOH	PCA	+192	+250	1.75	1600
07.29.81-2	O_2	NaOH	PCA	-310	-400	1.4	1600
07.29.81-3	H_2	NaOH	PCA	+155	+200	1.4	1600
07.29.81-4	H_2	H2SO4	PCA	+155	+200	1.4	1600
07.30.81-1	H_2	Na_2SO_4	PCA	+155	+200	1.4	1600

E. Incipient Gas Evolution On Vertical Electrodes

(1)	O_2	gold	360 mA/cm^2	NaOH 1 M
(2)	O_2	gold	360 mA/cm^2	NaOH 1 M & H_2SO_4 0.4 M
(3)	H_2	gold	180 mA/cm^2	NaOH 1 M & H_2SO_4 0.4 M
(4)	H_2	gold & nickel	180 mA/cm^2	NaOH 1 M
(5)	H_2	stainless steel	180 mA/cm^2	H2SO4 0.4 M & Na2SO4 2M

Note: This movie was presented at the fall meeting of the Electo- chemical Society, Denver, Colorado, in October 1981.

It is a selection of clips from sections B, C and D. The first sequence, on a full frame, showing oxygen evolution on gold in NaOH, demonstrates the events defined under 3.3.1. The next sequences are projected simultaneously, two at a time and side by side, using a split screen. The instants when the nucleation begins have been synchronized, so that an easier comparison of the growth stage can be made. A special emphasis is placed on coalescence, much more important in sulfuric acid than in the other two electrolytes.

3.3.2. Presentation of Results and Comments

3.3.2.1. The Diagrams

The above characteristics obtained from the movies are represented in the form of bar diagrams in the following figures:

Fig. 3.5.: The initiation time vs. parameters

Fig. 3.6.: The incipient growth time vs. parameters

Fig. 3.7.: The nucleation density vs. parameters

Fig. 3.8.: The average bubble size at detachement and in the bulk after one second.

On each of these figures, the volumetric gas evolution rate has a constant value of 1.25 $cm^3/cm^2 min$.

3.3.2.2. Hydrogen Evolution

The initiation time is low in sulfuric acid for all electrode materials; it is low in sodium hydroxide for gold only. When edge effects due to a nonuniform current distribution are observed, the value of Δt_1 is higher.

The nucleation density is high in sulfuric acid.

For this same electrolyte, the incipient growth time is generally short and the coalescence easy; the exception is on stainless steel, where the adherence is relatively strong even with ready coalescence.

In sodium sulfate also, the adherence is very low. The size of bubbles at detachement is therefore very small, and since coalescence is barely observed in this electrolyte, the bubbles in the bulk are also small.

This is not the case in sulfuric acid, where contact coalescence and scavenging coalescence occur readily; the average bubble diameter in the bulk after one second is then very big.

The influence of current density

The evolution of hydrogen on nickel in NaOH is observed for current densities ranging from 0.2 to 2 A/cm^2 (cf movies # 2.3.81.1 - 4). The general characteristics of the bubble layer under these conditions are:

- small bubbles
- low to medium ability to coalesce
- low to medium adherence.

The analysis of the movies was disturbed by a few problems:

- a bad distribution of the nucleation sites (i.e., of the current), especially at high current densities,
- a nonhomogeneous distribution of bubble size.

Nevertheless, some observations are possible (the figure 3.9. illustrates some of these effects):

- The nucleation density is a strong function of the current density.
- The initiwtion time and incipient growth time decrease with increasing the current density.
- The average size of bubble at detachement tends to increase with current density
- The bubble velocity increases asymptotically with current density.

3.3.2.3. Oxygen Evolution

A corrosion reaction takes place when nickel and stainless steel electrodes are used in sulfuric acid and, to a lesser extent, in sodium sulfate. This corrosion reaction uses part of the current. Therefore, the initiation time is longer and the incipient growth time and the nucleation density are not measurable with good accuracy.

In sodium hydroxide, there is no visible corrosion. In this electrolyte, the initiation time is lower for gold and steel than for nickel. In sodium hydroxide, the oxygen bubbles stay on the electrode

surface longer than in the other electrolytes. The nucleation density is always higher on gold.

Due to the low adherence and ready coalescence, the average bubble diameter is small at detachement and large after one second of electrolysis in sulfuric acid.

3.3.2.4. Comparison of Hydrogen and Oxygen Evolution

The nature of evolved gas has no profound influence on the initiation time. Nevertheless, on steel, the initiation time is longer for hydrogen than for oxygen; the nucleation density, in this case, is accordingly higher for oxygen.

The most obvious difference between hydrogen and oxygen evolution appears on diagram 3.6.: for any electrode/electrolyte system, the value of Δt_2 is always higher for oxygen than for hydrogen. In other words, the adherence of oxygen bubbles on any electrode surface is higher.

Furthermore, oxygen bubbles, both at detachement and after one second of electrolysis, are slightly larger than hydrogen bubbles. Sulfuric acid is an exception because of a corrosion reaction which complicates the process. The coalescence frequency is higher for O_2 than for H_2, in sodium hydroxide and in sodium sulfate.

3.4. Discussion

3.4.1. Initiation Time

For a volumetric flow rate of 1.25 $cm^3/cm^2 min$, the initiation time varies frome 10 to 100 ms (when no obvious corrosion occurs). Part of this time is used to charge the double layer. We can estimate the double layer charging time under our conditions:

$E = 2\ V$ $\qquad$ $C = 50 (K)\ 10^{-6}\ F/cm^2$

$j = 0.5\ A/cm^2$ $\qquad$ $t = R*C = C*E/j$

$t = 0.2\ ms$

Since the time necessary to charge the double layer is les than a millisecond, we can neglect it. Therefore, the initiation time is mainly used by the gas to reach the necessary supersaturation.

The concentration of dissolved gas at the electrode surface can be predicted by the relation [4]:

$$c = c_{bulk} + \frac{2j}{nF} \sqrt{\frac{t}{D}}\ \text{ierfc}\ \frac{x}{2\sqrt{Dt}}$$

with the conditions:

$c_{bulk} = 0$, $\qquad$ 2 ierfc(0) = 1.1284, we have:

$$c(x = 0) = 1.1284\ (j/nF)\ \sqrt{t/D}$$

For hydrogen and oxygen, the values of the current density and of the physical constants are the following:

	Hydrogen	Oxygen
Current density [A/cm^2]	0.2	0.4
Diffusivity [cm^2/s]	3.8×10^{-5} [4]	2.6×10^{-5} [30]
Solubility at 25°C [$mole/cm^3$]	8.5×10^{-7} [29]	14×10^{-7} [29]
The concentration of dissolved gas at the electrode surface is then given as a function of time (with time in seconds):		
$c(x = 0)$ [$mole/cm^3$]	$1.9 \times 10^{-4} \sqrt{t}$	$2.4 \times 10^{-4} \sqrt{t}$

For initiation time varying between 10 and 100 ms, the concentration of dissolved gas (e.g. the limiting gas concentration) is between 22 and 70 times the value of the saturation concentration for hydrogen and between 16 and 45-times that for oxygen. All these values are of the order of magnitude of Vogt's data [14].

It is to be noted that, due to the nonuniformity of the current distribution, the initiation-time data are perhaps questionable. The nucleation could have already begun on other portions of the electrode than the one observed.

3.4.2. Nucleation Density, Oxide Layer and Corrosion

The supersaturation concentration depends on the number of bubble nuclei at the surface. We can see this dependence in the movies in which the nonuniformity of the current distribution is not inordinately high; the higher the nucleation density, the lower the supersaturation value, hence the lower the initiation time. The nonuniformity of the current distribution is manifest in some of the movies during the nucleation time; nucleation begins on the lateral edges of the frame, then propagates over the surface (see movie 3.8.81-1). When the current

distribution is very uniform, bubble nuclei appear simultaneously throughout the surface. The Wagner number characterizes the degree of uniformity of the current distribution.

The nucleation density depends upon, among other things, the nature and preparation of the surface. For example, the anodic prepolarization before oxygen evolution multiplies the nucleation density by a factor of 100. This is seen in movie A.

The anodic polarization of a metallic electrode causes the formation of an oxide layer on its surface, more or less stable depending on the nature of the metal and of the electrolyte. The tendency to corrode is higher at low pH. For example, the evolution of oxygen on stainless steel and nickel electrodes in Na_2SO_4 and H_2SO_4 electrolytes competes with a parasitic corrosion reaction. We should therefore be very cautious in the interpretation of the data taken under these conditions. On the other hand, the corrosion reaction does not exist or is very slow on gold in every electrolyte studied as well as on stainless steel and nickel in sodium hydroxide. The oxide layer has a very strong effect on the characteristics of the bubble evolution, particularily on the nucleation density. Beginning from a bare metallic surface, the nucleation density is very low and increases with time because of the oxide formation. If the electrode is positively polarized in a previous solution, then the nucleation density is very high. The prepolarization of the electrode creates an oxide layer at its surface; if no prepolarization is done, this oxide layer is formed during the incipient bubble evolution and consumes part of the current. If the corrosion effects are ignored, the presence of the oxide layer results in a shorter ini-

tiation time and a higher nucleation density. On the other hand, the corrosion reaction tends to promote:

- a longer initiation time
- a higher nucleation density due to the etching of the surface.

3.4.3. Incipient Growth Period

After nucleation, the bubbles grow homogeneously by diffusion of dissolved gas to a certain number of sites. But after a certain time, they begin to interact and to coalesce. Several different types of coalescence can occur on the electrode surface:

- contact coalescence of homogeneous bubbles,
- radial attraction coalescence of bubbles differing in size,
- scavenging coalescence (the scavenging of small bubbles by large bubbles sliding upward along a vertical electrode).

The general effect of the coalescence is to increase the free electrode surface and therefore decrease the electrical resistance of the cell. Coalescence occurs more or less readily depending on certain properties such as electrolyte viscosity and bubble surface tension. The last two types of coalescence occur when all the events of the gas evolution appear simultaneously, i.e., when the bubble layer is not homogeneous. During the incipient growth period, only the first type of coalescence, the contact coalescence, occurs. The effect of this coalescence is a decrease in the number density n and an increase of the bubble size. The larger resulting bubbles remain on the surface and continue to grow until new coalescence occurs with their neighbors.

Eventually, the critical size for detachement is reached, the whole bubble layer leaves the surface, and new bubble nuclei appear on it. The case of growth by diffusion of one bubble is described by Scriven [31]; its radius varies with the square root of the time. In the case of a population of interacting bubbles, the diffusion process is only slightly responsible for the growth of bubbles, because of coalescence. More than 80 percent of the growth can then be due to coalescence. During the incipient growth period, a single bubble can coalesce more than ten times before leaving the surface. After coalescence, the resulting bubble oscillates at a frequency of 2000 Hz. This oscillation can trigger coalescence between bubbles in its vicinity.

3.4.4. Detachement Time

In the case of non-interacting bubbles growing reversibly, their size at detachement is determined by their contact angle with the electrode surface. This contact angle depends on the surface tension, which in turn is a function of the electrode potential [32]. Therefore, as a function of the potential, the contact angle most probably behaves according to the electrocapillary curve: an anodic or cathodic potential decreases the value of the contact angle. Furthermore, any adsorbed species on the electrode decrease the surface tension and therefore decrease the contact angle of the attached bubbles. At constant potential, raising the concentration of electrolyte decreases the contact angle; raising the current density achieves the same effect.

For a uniform current distribution, all the bubbles leave the surface at the same time. This is not always the case, and again the edge

effects are visible: bubbles on the lateral edges leave the surface before the bubbles in the center of the frame.

3.4.5. Transition Period

After the detachement of the first generation of bubbles, new nuclei appear. But due to their interaction with the rising bubbles, their behavior is no longer the same. Generally, they are scavenged before they reach their critical size for detachement. Of course, the choice of location of the observed portion of the electrode is now important; if we look at the very bottom of the electrode, we will see the evolution of the successive generations more distinctly and it will be a longer time before the events become random (cf movies with PSB).

4. The Resistance of the Bubble Layer

4.1. Introduction

One of the effects of gas evolution in electrolysis is the rise in resistance of the electrolyte due to obstruction by bubbles. These can be classified either as bubbles attached to the electrode or bubbles in the electrolyte bulk.

With a judicious choice of cell geometry (e.g., gas diverting electrode [18], inclined sectioned electrodes [19]), most of the bubbles in the bulk can be circumvented. Therefore, the overall increase in electrical resistance due to bubbles can be largely attibuted to the attached surface bubbles. The purpose of this section is to measure the resistance due to the bubble layer at the electrode surface. In order to compare the visual information obtained from the movies with the value of the resistance, the dependence of resistance on time is established during the short period (500 to 1000 ms) following the onset of current.

4.2. Principles of the Method

The electrical resistance between the working and reference electrode is measured as a function of the time of electrolysis. For this purpose, a current interrupted technique is used [33]. The current is allowed to flow for a defined time and then is switched off. During that time, the voltage is recorded on a fast-writing storage oscilloscope, with a resolution of one microsecond. The ohmic contribution to the voltage drop disappears almost instantaneously (in less than 10^{-12} seconds); the electrode potential decay is much slower (a few millivolts

per microsecond). It is therefore possible to separate the ohmic drop from the electrode potential. Recording the current jump at the same time allows calculation of the resistance between working and reference electrodes. Nonuniform current distribution on the working electrode and/or a non uniformly charged double layer would lead to erroneous results: particular attention must be directed to the cell geometry to avoid these problems.

4.3. Experimental

4.3.1. The Cell

Figure 4.1. shows the resistance cell. Made of Lucite, it is filled with a stagnant electrolyte and contains two facing vertical electrodes: the working electrode on the right and the counter electrode on the left. The active surface of each is 8.06 cm^2. Between them, and covering the entire cross-section, is a platinum grid (80 mesh, 10% rhodium) which serves as a reference electrode. It is held in position by two slits in the walls of the cell.

The temperature is measured after every run and introduced in a correcting expression for the conductivity, which is strongly dependent on the temperature. The experiments are conducted at room temperature, but as the electrolysis proceeds, the temperature rises from Joule heating and consequently must be measured. This measurement is made at the counter electrode surface with a thermocouple for which the temperature/voltage relation is:

$$T[^{o}C] = 25\ E\ [V] + 0.4$$

The working electrode is interchangeable: plain stainless steel, plain nickel and electroplated gold on nickel (50 microns) are used. The counter electrode is made of stainless steel. For these experiments, an aqueous solution of sodium hydroxide is used. This electrolyte is poured in and pumped out through small holes at the top of the cell.

4.3.2. The Apparatus

Figure 4.2. shows a schematic representation of the experimental set-up. Figure 4.3. shows the function of each device and the connections. On the main circuit between the power supply and the cell are the following devices:

(1) a set of mercury-wetted relays

(2) a field-effect transistor

(3) a 100-ohm resistor

The relays (1) close the circuit during the period $\Delta t_a + \Delta t_b$. They are activated by a signal of +5 V, provided by the potentiostat/galvanostat (8) used in galvanostatic mode. The field-effect transistor (2) has a very fast response (less than a nanosecond); its role is to switch off the current for a short period Δt_c (roughly 1 ms), just after the period Δt_a. It is controlled by a potential pulse of 5 V from the function generator (7). The electrical current is measured through the 100 ohm resistor (3).

Current and voltage drops are recorded at that moment by the oscilloscope (9). The time interval, Δt_a, is varied from 10 ms to 1000 ms; for every new time set, the measurement of current and voltage drops is made in a new solution.

4.4. Operating Mode and Treatment of Data

The current is interrupted after a certain time of electrolysis, Δt_a. This time is varied over a range from 10 ms to 1000 ms, which allows construction of the resistance versus time profile for the incipient gas evolution. Generally, the measurements are made for decreasing values of Δt_a from 500 ms to 10 ms, then for increasing values of Δt_a from 400 ms to 1000 ms.

For every set value of Δt_a, the following characteristics are measured:

- the current I [A]
- the voltage drop ΔE [V]
- the electrode surface temperature T [^{o}C]

The conductivity k of the electrolyte is a function of the temperature:

for 0.1 M NaOH, $k = (2.84\ T + 150.2) \times 10^{-4}$ mho/cm (= 0.02212 at 25 ^{o}C)

for 1 M NaOH, $k = (3.04\ T + 103.2) \times 10^{-3}$ mho/cm (= 0.179 at 25 ^{o}C).

Introducing the correction factor for the temperature variations, the electrical resistance at T = 25 ^{o}C is obtained as followed:

$$R = [k(T)/k(25^{o}C)][\Delta E/I]$$

The resistance of the electrolyte in the absence of bubbles, R_o, is obtained for a very short duration of electrolysis (approximately 10 ms). For higher values of Δt_a, the resistance of the electrolyte in the presence of bubbles, R_t, is recorded. These bubbles are growing with time.

The results are expressed graphically as follows:

$$R^* = f(t) \quad , \quad \text{where } R^* = (R_t - R_o)/R_o$$

The profile of the resistance is expected to be the following (cf. figure 4.4.):

1) initiation period, during which the necessary supersaturation is built up; no bubbles, and hence no resistance increase.

2) incipient growth period: for a single bubble, Scriven [31] calculated a square-root dependance of the growth rate on the radius. On the other hand, Sides [6] found that the increase in resistance is proportional to the cube of the radius. This corresponds to a $t^{3/2}$-dependance for the resistance increase. This relation is valid for a single bubble, or for bubbles which do not interact. For a population of interacting bubbles, the resistance increase will be larger, and will be influenced by the coalescence frequency.

3) transition period: the resistance profile exhibits a maximum, depending on the respective residence times of the bubbles at the electrode surface and in the bulk.

4) steady state: the resistance of the cell is constant when the gas generation rate is equal to the rate of the gas reaching the electrolyte surface.

4.5. Results

4.5.1. The Early Experiments

The early experiments were performed in 0.1 M NaOH solutions. They were marked by the search for conditions which would give reproducible measurements.

Their results show that the preparation of the electrode surface is very important: the electrochemical treatment must be made as carefully as the mechanical treatment (see 3.2.1.).

The electrode surfaces are generally active when polarized, and a steady state of these surfaces must be reached before making any measurement. This is obtained by a long prepolarization of the same sign as during the measurement run.

The history of the electrode and the operating mode for taking data have a big influence on the results. For example, in the case of oxygen evolution on gold or on stainless steel, a peak is present when the data are taken for increasing values of time. If a decreasing mode is used, this peak does not appear (cf. figure 4.5.).

Because of the formation of different layers on the electrode surface, the measured resistance without bubbles, R_o, is not the same for hydrogen evolution as for oxygen evolution. This problem will be considered later.

When comparing the respective resistance for O_2 and H_2 evolution on the same electrode during the growth period, we notice that the value of R^* is always higher for O_2 than for H_2. The analysis of movies does not

provide supporting evidence for such a difference. In fact, we have found that this difference is due to the low sodium hydroxide concentration. In this electrolyte, the change of the pH in the diffusion layer as the electrochemical reaction goes on is important and affects substantially the electrical conductivity in the vicinity of the electrode surface. Hydrogen and oxygen evolution produce OH^- and H^+ ions respectively. For our experimental conditions (G = 1.75 cm/min, 0.1 M NaOH), the potential drop due to the change in conductivity can be more than 30 percent of the total drop.

If 1 M NaOH is used under the same conditions, this effect is much smaller (less than 3.5 percent of the measured drop) and can be then neglected. (See appendix for the estimate of this potential drop.) Therefore, the next measurements are done using 1 M NaOH.

4.5.2. The Experiments in 1 M NaOH

Two series of measurements were made in 1 M NaOH on three different electrodes:

Series 1: G = 1.75 cm/min for gold, nickel and stainless steel
Series 2: G = 1.25 cm/min for gold and nickel and
G = 1.40 cm/min for stainless steel

Because the value of R_o was not constant from run to run (see table 4.1.) the reduced resistance R* is calculated from an average value of R_o, R#. The following steps explain the data reduction:

(1) $R = f(t)$

(2) $\Delta R = f(t)$, where $\Delta R = R_t - R_o$

(3) $R\# = \sum_n \frac{R_o,n}{n}$

(4) $R^* = \Delta R / R\#$

Table 4.1.: The values of R_o (in mohm) for the different runs.

Series	Gas	Gold	Nickel	St. Steel	R# [mohm]
1	H_2	200	210	200	197 +/-15
1	O_2	220	180	176	
2	H_2	195	207	195	195 +/-8
2	O_2	200	195	180	

The results of the resistance measurements are presented graphically in figure 4.6.

The different periods are discernable: initiation, incipient growth, transition and steady state. The precise moment of detachement was obtained from the movies. The resistance at detachement is always higher for oxygen. There is no significant difference in the resistance profiles among the various electrode materials, but the nature of the gas evolved does influence these profiles. The resistance increase across the growing bubble layer does not differ greatly between hydrogen and oxygen evolution. Nonetheless, at steady state, the resistance is consistently higher for oxygen. This can be related to the high adherence observed for oxygen bubbles on the surface. During the transition

period of hydrogen evolution, the observed maximum in the resistance profile may be due to the accumulation of small bubbles in the solution before the onset of the fluid motion. If the residence time of bubbles in the bulk is longer than the residence time on the electrode surface, the transition time will be rather long.

To improve the measurements, several problems still need to be solved, particularily for the determination of the value of R_o. In our case, the value of R_o is found to depend on the nature of the evolved gas. This may be due to additional resistances included in the measured values under certains conditions. For example, an oxide layer on the gold electrode during O_2 evolution could explain the higher value for R_o; but this explanation could not hold for the case of nickel or stainless steel, because the value of R_o measured when hydrogen is evolved is higher.

The movies show dramatic differences between gas evolution in sulfuric acid and sodium hydroxide. Unfortunately, good resistance-increase data are available only in sodium hydroxide. The experiments in acid lead to corrosion problems, which have not yet been circumvented.

5. Theoretical Models and Their Verification

5.1. Introduction

Many investigators have developed theoretical models for predicting the conductivity of heterogeneous media. However, the case of the gas layer on the electrode surface was not considered in itself before Sides' work. In his thesis [5], he reviewed many of these models and evaluated their applicability to this special case. He experimented with planar arrays of spheres which simulate bubble layers on electrodes. This chapter treats experimental data from actual bubble layers, taken during the incipient growth period, and compares them with the favored models.

5.2. Choice and Description of Models to be Tested

From his simulation measurements, Sides concluded that the Distribution model [34] and Meredith's equation [35] are not grossly in error when applied to a bubble layer. He did however develop a model to describe the resistance specifically across a layer of bubbles, the Constriction model [5].

The Distribution model and the Constriction model will be considered for testing (see figure 5.1.).

The Distribution model was developed by Meredith and Tobias for random arrangements of multisized spheres. It is generally suitable for use in the bulk. The conductivity ratio is expressed versus the volume void fraction.

The Constriction Model, as indicated by its name, is based on the constriction of the current across a planar hexagonal array of bubbles.

It is assumed that the current distributes itself evenly throughout the available electrolyte present among the bubbles. Here, the conductivity ratio is given as a function of the electrode coverage.

5.3. Experimental

A separate observation cell (variation PCA) is used, which is specially designed to have an even current distribution. During the incipient growth period, the average number density n and the average bubble diameter d were measured over time. The layer thickness during this period is taken as the average bubble diameter.

From the average number density and layer thickness, we can calculate the electrode coverage as well as the void fraction:

- electrode coverage, f = projected area of bubbles / total area

$$= n \pi d^2 / 4$$

- void fraction, θ = bubble volume / layer volume

$$= n \pi d^2 / 6$$

The conductivity ratio is defined as:

k^* = bubble layer conductivity / electrolyte conductivity

$= k_b / k_o$

The resistance measurements give us the value of R^* as a function of time. This value is obtained for a given gap between working and reference electrode. This gap width, l, can be calculated from the measured R_o value by the expression:

$l = k_o R_o A_w$ where A_w is the electrode surface area.

For a bubble layer of thickness d (measured from the movies) in a cell with interelectrode spacing l, the total resistance can be expressed by the relation:

$$R_t = (1 - d^*) C / k_o + d^* C / k_b \qquad \text{with} \qquad d^* = d / l$$

The transformation relation between k^* and R^* is therefore the following:

$$k^* = d^* / (R^* + d^*)$$

The movie # 07.13.81-2 and the resistance profile on stainless steel in series 1 (figure 4.7.c) have been obtained under identical experimental conditions:

- electrode: stainless steel
- electrolyte: 1 M NaOH
- gas evolved: oxygen
- current density: -500 mA/cm^2
- gas generation rate, G: 1.75 cm/min

The movie speed was 870 fps. The interelectrode gap, l, in the resistance experiment was 0.28 cm.

The variation of the number density and of the average diameter of the bubbles appears on figure 5.2.

5.4. Results

5.4.1. Comparison of Calculated and Measured Gas Evolution Rates

During the incipient bubble growth period, the volume of gas generated per unit area of electrode surface is determined from measurements as follows:

$$V_m = n \pi d^3 / 8$$

This volume can be calculated, on the other hand, for a given current density and assuming 100 percent current efficiency, by Faraday's law:

$$V_c = j V\# t / zF$$

The ratio V_m/V_c is reported as a function of the time on figure 5.3. for the above conditions. This plot shows relatively good agreement between calculated and measured volumes, except at the beginning, where most of the gas generated remains in solution and builds up the necessary supersaturation for nucleation.

During most of the incipient growth period, all of the generated gas goes into the bubbles. These result reflects a uniform current distribution in this case.

R.A. Putt [1] did the same comparison for the evolution of hydrogen on nickel, but he never found a value of V_m/V_c higher than 0.3. This discrepancy between our conclusions and those of Putt can be explained two ways:

1) The behaviour of hydrogen may be different from that of oxygen; this is not expected as the diffusion coefficients and solubilities are quite similar for the two gases.

2) The cell used by Putt may not give a uniform current distribution.

5.4.2. Verification of Models

The data obtained are compared with the predictions from chosen models in figure 5.4. The result is quite satisfactory, considering the numerous experimental difficulties; the diagram shows clearly that each of the tested models suitably predicts the conductivity of the incipient bubble layer. The electrode coverage is seen to be the most important factor influencing this conductivity. This factor, calculated from the number density and the average diameter of the bubbles, depends on coalescence frequency. When the conductivity over the whole cell is considered, the layer thickness must also be included.

From the success of the models and the knowledge of the bubble layer thickness, we now know quantitatively how the resistance of a cell rises with the electrode coverage. To minimize the resistance of a gas-evolving cell, both the electrode coverage and the bubble layer thickness should be lowered. Strong coalescence achieves both of these desired effects. This leads to the conclusion that it is advantageous to operate under conditions for which coalescence readily occurs, as in our experiments in sulfuric acid. In this light, it appears worthwhile to conduct further studies of this type on bubble dynamics, particularly on coalescence phenomena.

Bibliography

[1] W. C. Hui, M.S. thesis, University of California, LBL Report No. 11945 (1980)

[2] C.W. Tobias, J. Electrochem. Soc, 106 (1959) 833

[3] H.Y. Cheh, Ph.D. thesis, University of California UCRL Report No. 17324 (1967)

[4] C.K. Bon, M.S. thesis, University of California, UCRL Report No. 19612 (1970)

[5] P. J. Sides, Ph.D. thesis, University of California, LBL Report No. 11849 (1980)

[6] P. Sides, C. Tobias, J. Electrochem. Soc., 127 (1980) 288

[7] W. C. Hui, M.S. thesis, University of California, LBL Report No. 11945 (1980)

[8] R. Piontelli, B. Mazza, P. Pedeferri, A. Tognoni Electrochimica Metallorum, 2 (1967) 257 - 436

[9] B. Mazza, P. Pedeferri, G. Re, Electrochimica Acta, 23 (1978) 87

[10] Proceedings of the International Colloquium on Drops & Bubbles Cal. Tech. + Jet Prop. Lab, August 28 - 30, 1984

[11] F. Hine, K. Murakami, J. Electrochem. Soc., 127 (1980) 292

[12] F. Hine, K. Murakami, J. Electrochem. Soc., 128 (1981) 64

[13] H. Vogt, Electrochimica Acta, 23 (1978) 1019

[14] H. Vogt, Electrochimica Acta, 25 (1980) 527

[15] H. Vogt, Electrochimica Acta, 26 (1981) 1311

[16] R. Alkire, Po-Yen Lu, J. Electrochem. Soc., 126 (1979) 2118

[17] H. Hamzah, A. Kuhn, J. Appl. Electrochem., 10 (1980) 635

[18] J. Jorne, J. Louvar, J. Electrochem. Soc., 127 (1980) 298

[19] G. Kreysa, H.-J. Kuelps, J. Electrochem. Soc., 128 (1981) 979

[20] L. Janssen, Electrochimica Acta, 23 (1978) 81

[21] L. Janssen, E. Barendrecht, Electrochimica Acta, 24 (1979) 693

[22] N. Ibl, C. Venczel, Metalloberflaesche, 24 (1970) 365

[23] L. Janssen, S. van Stralen, Electrochimica Acta, 26 (1981) 1011

[24] C. Iwakura, M. Inai, T. Uemura, Tamura, Electrochimica Acta, 26 (1981) 579

[25] D. Denton, J. Harrison, R. Knowles, Electrochimica Acta, 26 (1981) 1197

[26] H. Medwin, "Counting Bubbles Acoustically : a Review" Ultrasonics, January 1977

[27] "High speed photography" Eastman Kodak Comp (1975) SBN 0 - 87985 - 165 - 1

[28] Photomethods, 24(5), (1981)

[29] CRC Handbook, 56th edition (1976)

[30] R. Reid, T. Sherwood, "The properties of gases and liquids" Mc Graw-Hill Book Company, N.-Y. (1958)

[31] L. Scriven, Chem. Eng. Sci., 10 (1959) 1

[32] B. Kabanow, A. Frumkin, Zeit. fuer Phys. Chem., 165A (1933) 433

[33] J. McIntyre, W. Peck, J. Electrochem. Soc., 117 (1970) 747

[34] R. E. Meredith, C. W. Tobias, J. Electrochem. Soc., 108 (1961) 286

[35] R. E. Meredith, C. W. Tobias, J. Appl. Phys., 31 (1960) 1270

Figure Captions

Fig. 3.1. : The observation cell with the three variations

Fig. 3.2. : Comparison of the conductivity and relative viscosity of the electrolytes

Fig. 3.3. : Schematic of observation aparatus (top view of the cell)

Fig. 3.4. : The sequence of events

Fig. 3.5. : Initiation time for various electrolytes, electrode materials and evolved gases

Fig. 3.6. : Incipient growth time for various electrolytes, electrode materials and evolved gases

Fig. 3.7. : Estimate of the nucleation density for various electrolytes, electrode materials and evolved gases

Fig. 3.8. : Average bubble diameter for various electrolytes, electrode materials and evolved gases

Fig. 3.9. : Influence of the current density on the rate of events

Fig. 4.1. : The resistance cell 1: reference electrode
2: working electrode

Fig. 4.2. : Schematic of the resistance experiments set-up

1 : set of mercury-wetted relays

2 : field-effect transistor

3 : 100-ohm resistor

4 : resistance cell

5 : power supply DC, Perkin Electronics, 50V/40A

6 : universal programmer PAR 175

7 : function generator Interstate F-77

8 : potentiostat Amel 551

9 : 2-channel oscilloscope Nicolet 1090A Explorer

Fig. 4.3. : Function of devices and connections

Fig. 4.4. : The elements of the resistance profile

Fig. 4.5. : Resistance profile in an unchanged electrolyte

Oxygen evolution on stainless steel in 0.1 N NaOH

l = 0.46 cm G = 1.75 cm3/cm2 min
o : without prepolarization, forward
x : with anodic prepolarization, or backward

Fig. 4.6. : The resistance profiles

Fig. 5.1. : The theoretical effective conductivity models

Fig. 5.2. : Variation of the number density and of the average diameter of bubbles during the incipient growth.

Oxygen evolution on stainless steel in 1M NaOH
G = 1.75 cm3/cm2min (movie # 7.13.81-2)

Fig. 5.3. : Comparison of measured and calculated volume of generated gas.

Oxygen evolution on stainless steel in 1M NaOH
G = 1.75 cm3/cm2min (movie # 7.13.81-2)

Fig. 5.4. : Comparison of the effective conductivity models with the experimental data

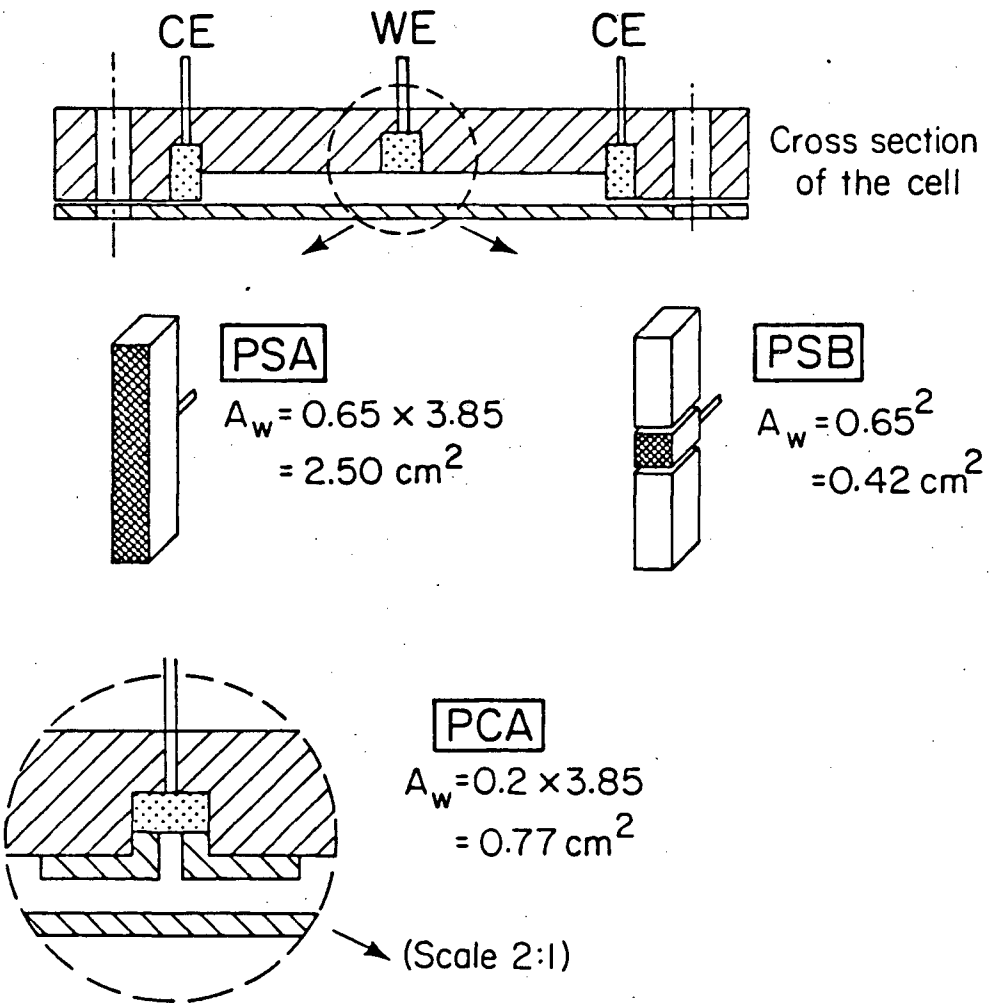
CE
WE
CE
Cross section of the cell
PSA
$A_w = 0.65 \times 3.85$
$= 2.50\ cm^2$
PSB
$A_w = 0.65^2$
$= 0.42\ cm^2$
PCA
$A_w = 0.2 \times 3.85$
$= 0.77\ cm^2$
(Scale 2:1)
XBL 8111-1636

Fig. 3.1

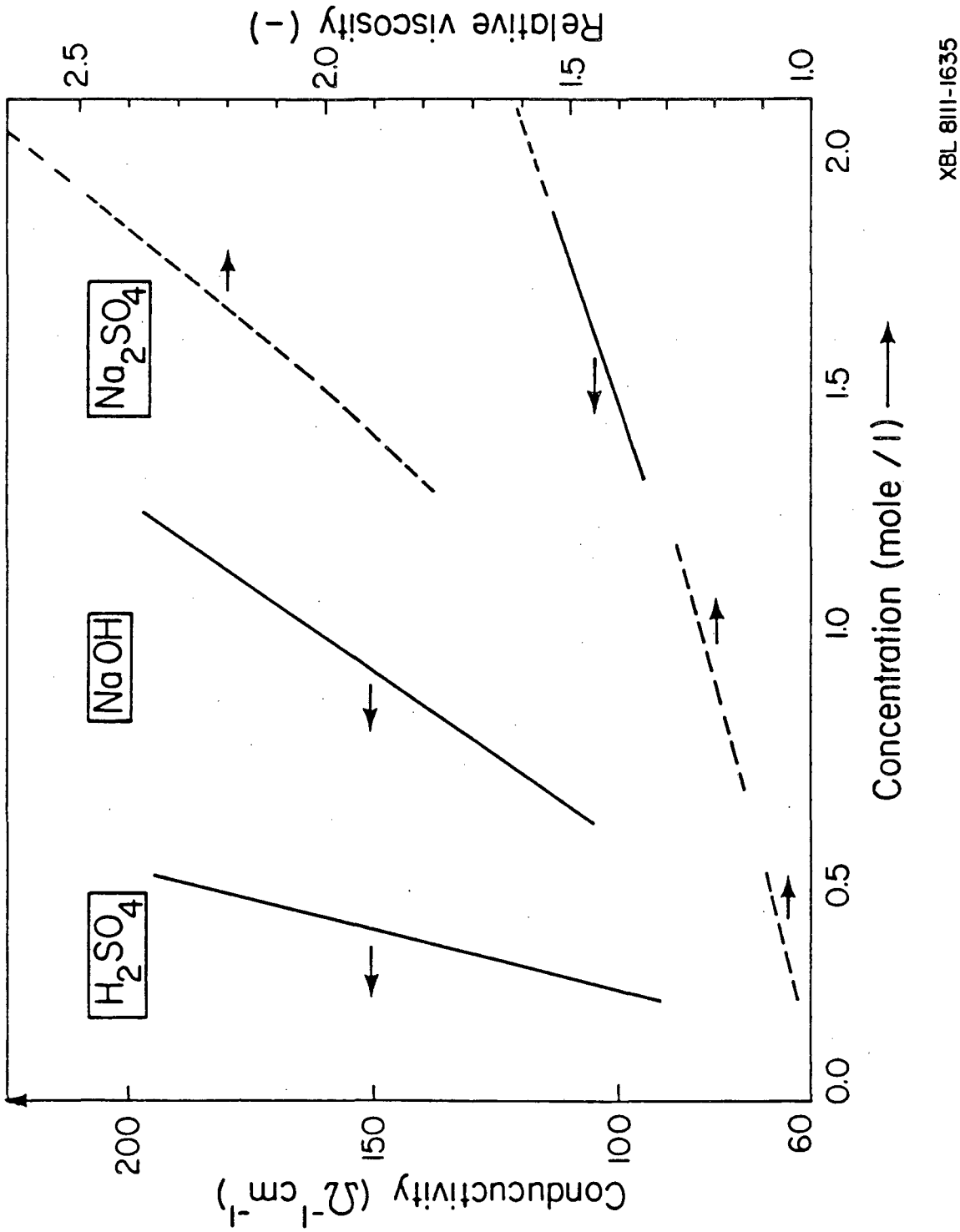

XBL 8111-1635

Fig. 3.2

Schematic of Observation Apparatus (Top View of the Cell)

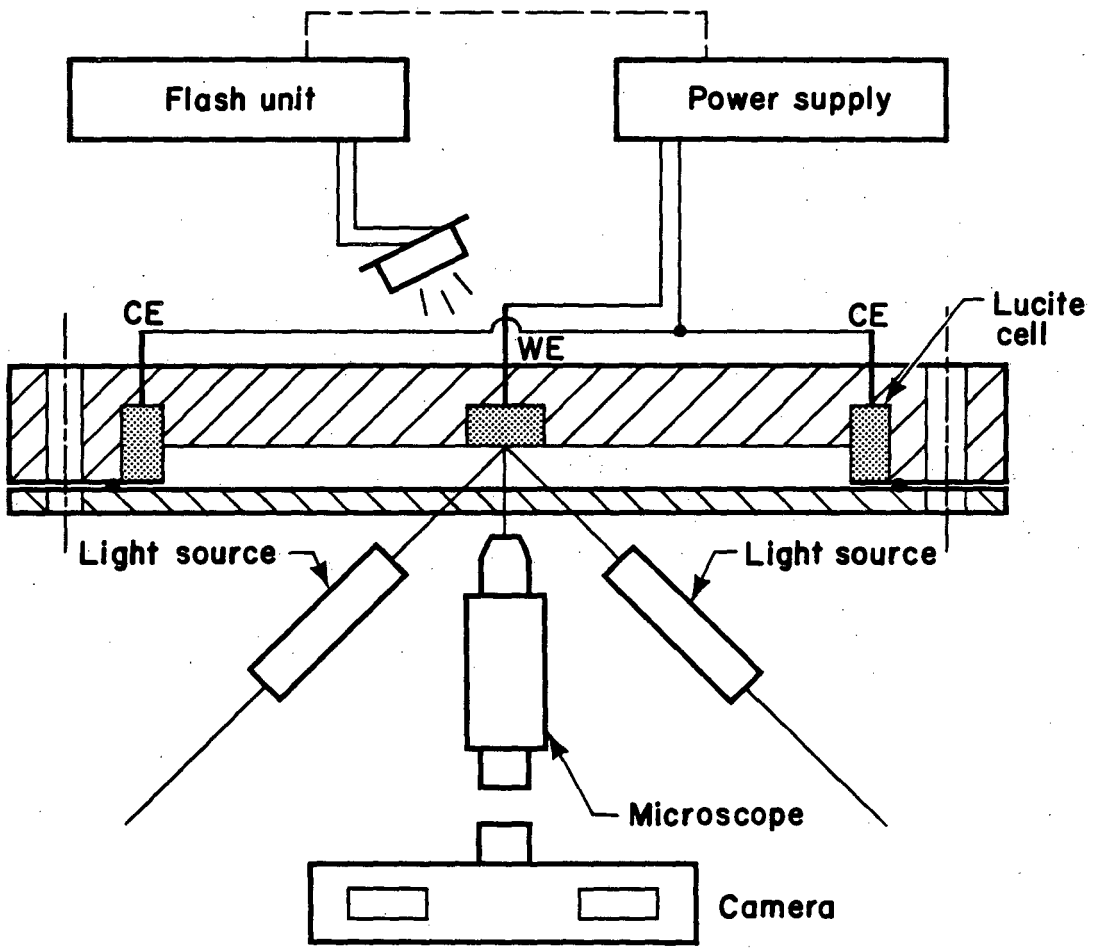

XBL 819-1312

Fig. 3.3

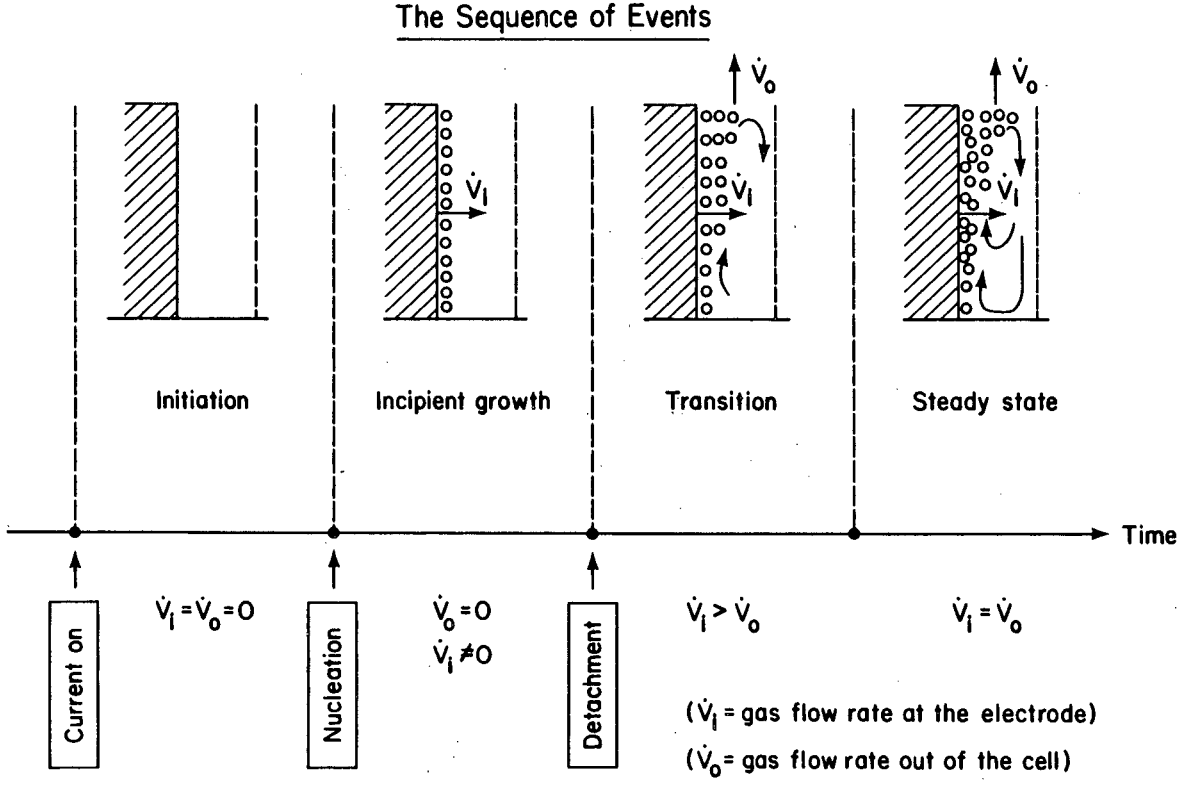
The Sequence of Events
$\dot{V}_o$
$\dot{V}_i$
Initiation
Incipient growth
Transition
Steady state
Time
Current on
$\dot{V}_i = \dot{V}_o = 0$
Nucleation
$\dot{V}_o = 0$
$\dot{V}_i \neq 0$
Detachment
$\dot{V}_i > \dot{V}_o$
$\dot{V}_i = \dot{V}_o$
($\dot{V}_i$ = gas flow rate at the electrode)
($\dot{V}_o$ = gas flow rate out of the cell)
XBL 819-1315

Fig. 3.4

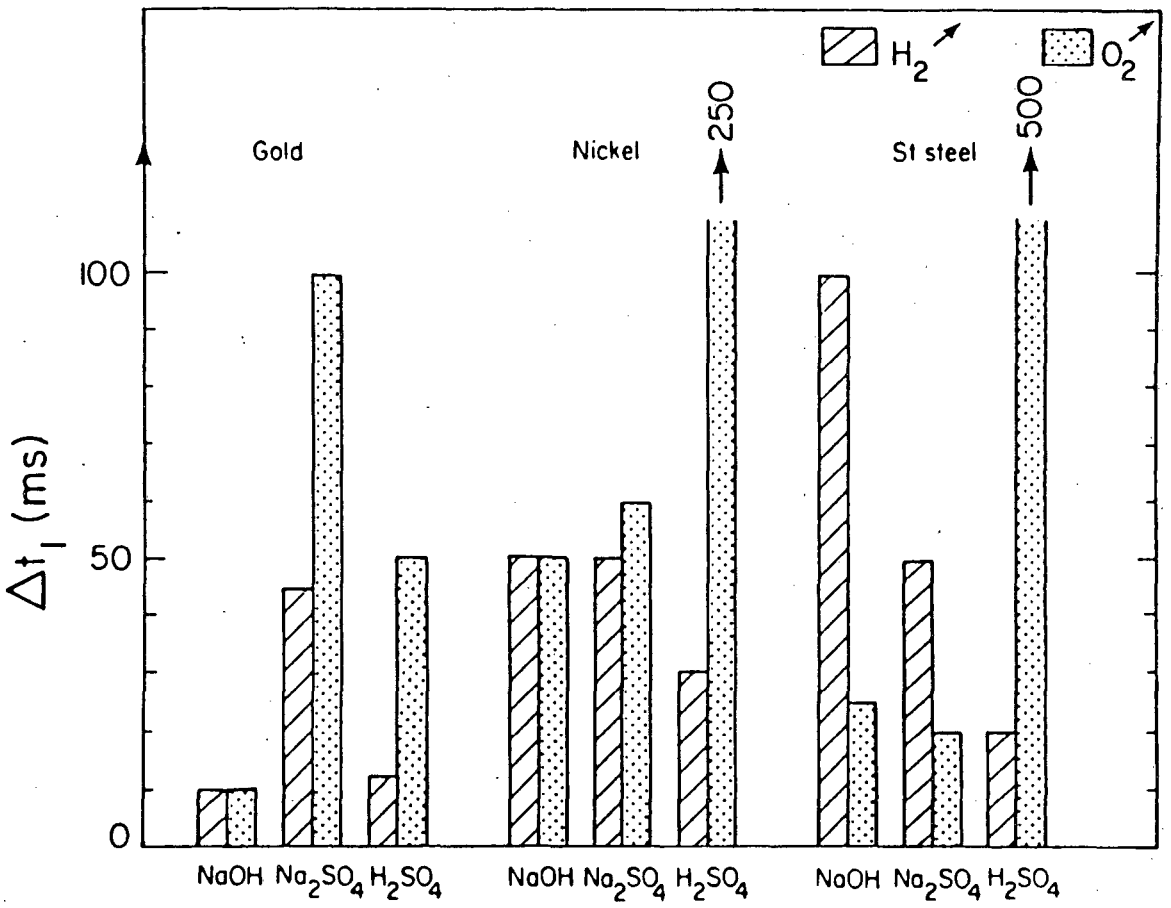

XBL 8111-1637

Fig. 3.5

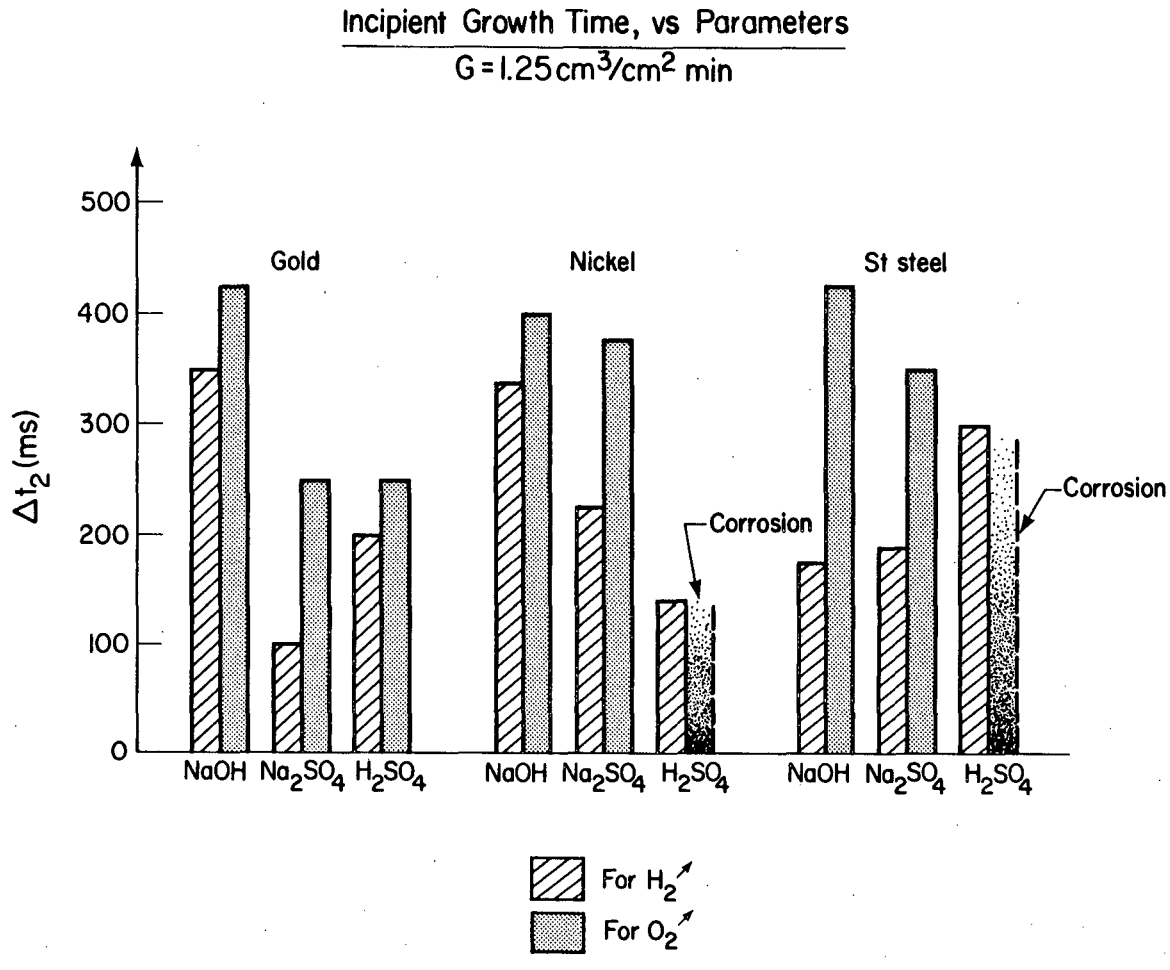
Incipient Growth Time, vs Parameters
G = 1.25 cm³/cm² min
Δt₂ (ms)
500
400
300
200
100
0
Gold
Nickel
St steel
Corrosion
Corrosion
NaOH
Na₂SO₄
H₂SO₄
NaOH
Na₂SO₄
H₂SO₄
NaOH
Na₂SO₄
H₂SO₄
For H₂
For O₂
XBL 819-1314

Fig. 3.6

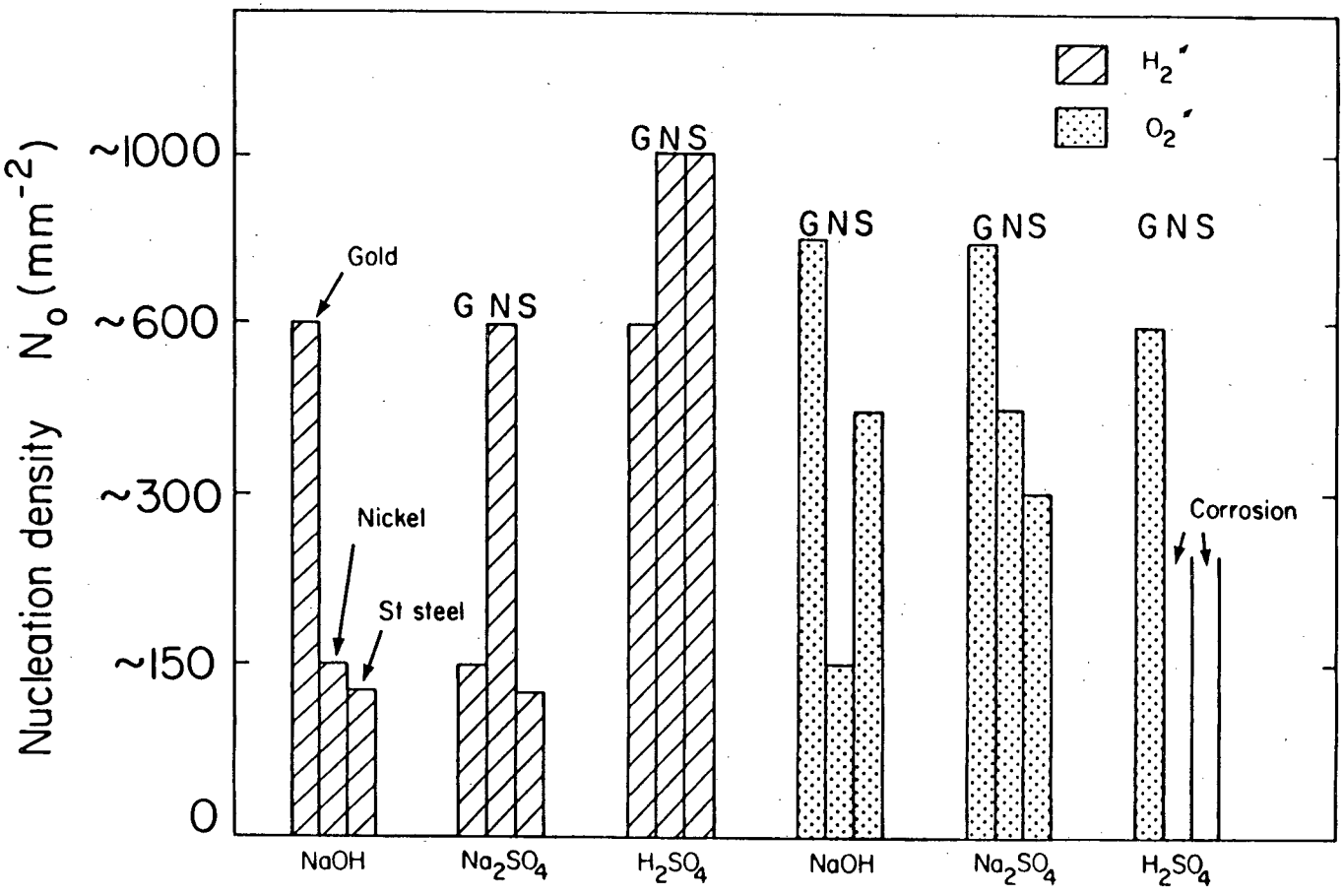
Nucleation density N_o (mm^{-2})
~1000
~600
~300
~150
0
H_2
O_2
Gold
Nickel
St steel
G N S
G N S
G N S
G N S
G N S
Corrosion
NaOH
Na_2SO_4
H_2SO_4
NaOH
Na_2SO_4
H_2SO_4
XBL 8111-1638

Fig. 3.7

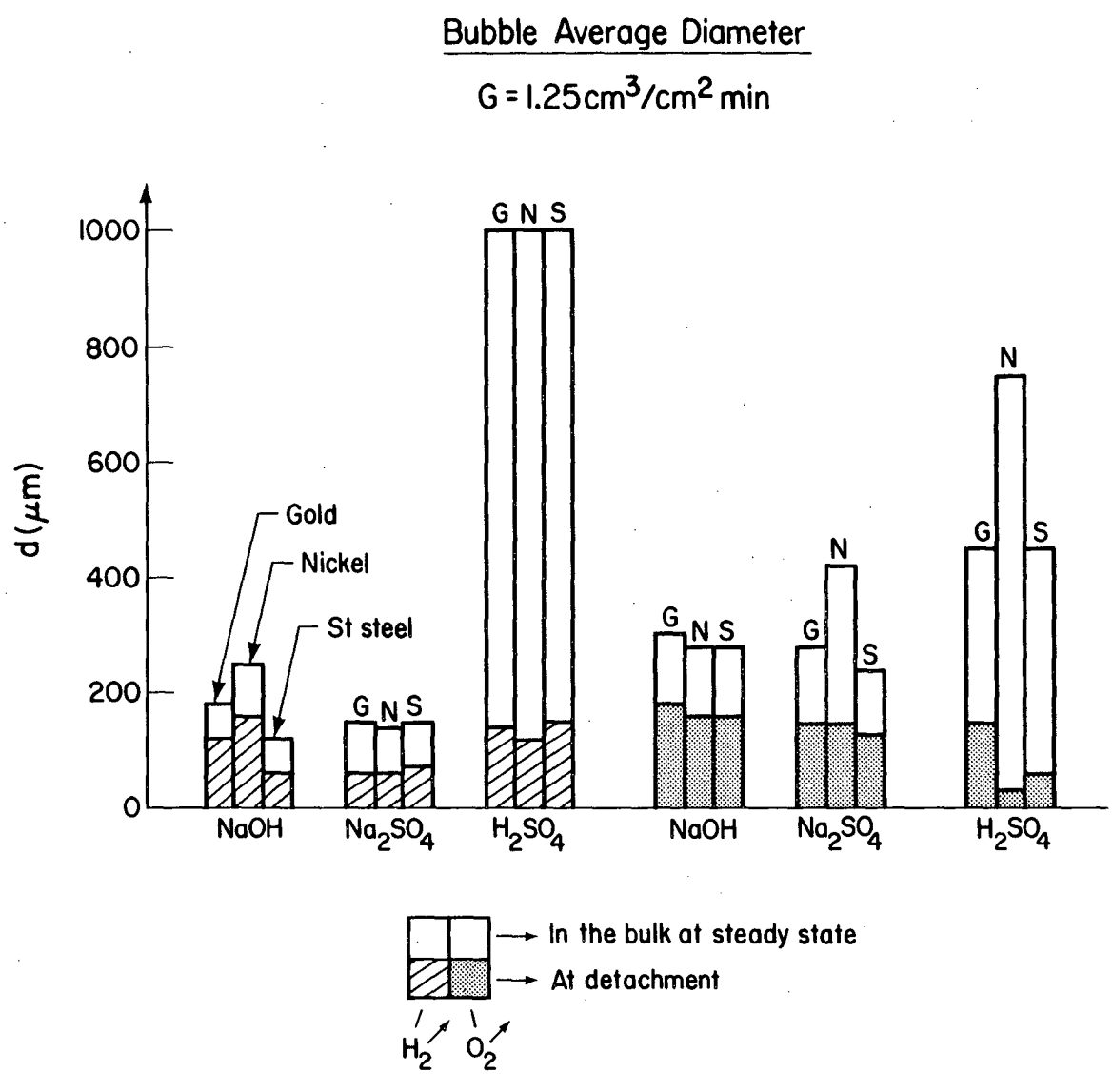

Fig. 3.8

XBL 819-1313

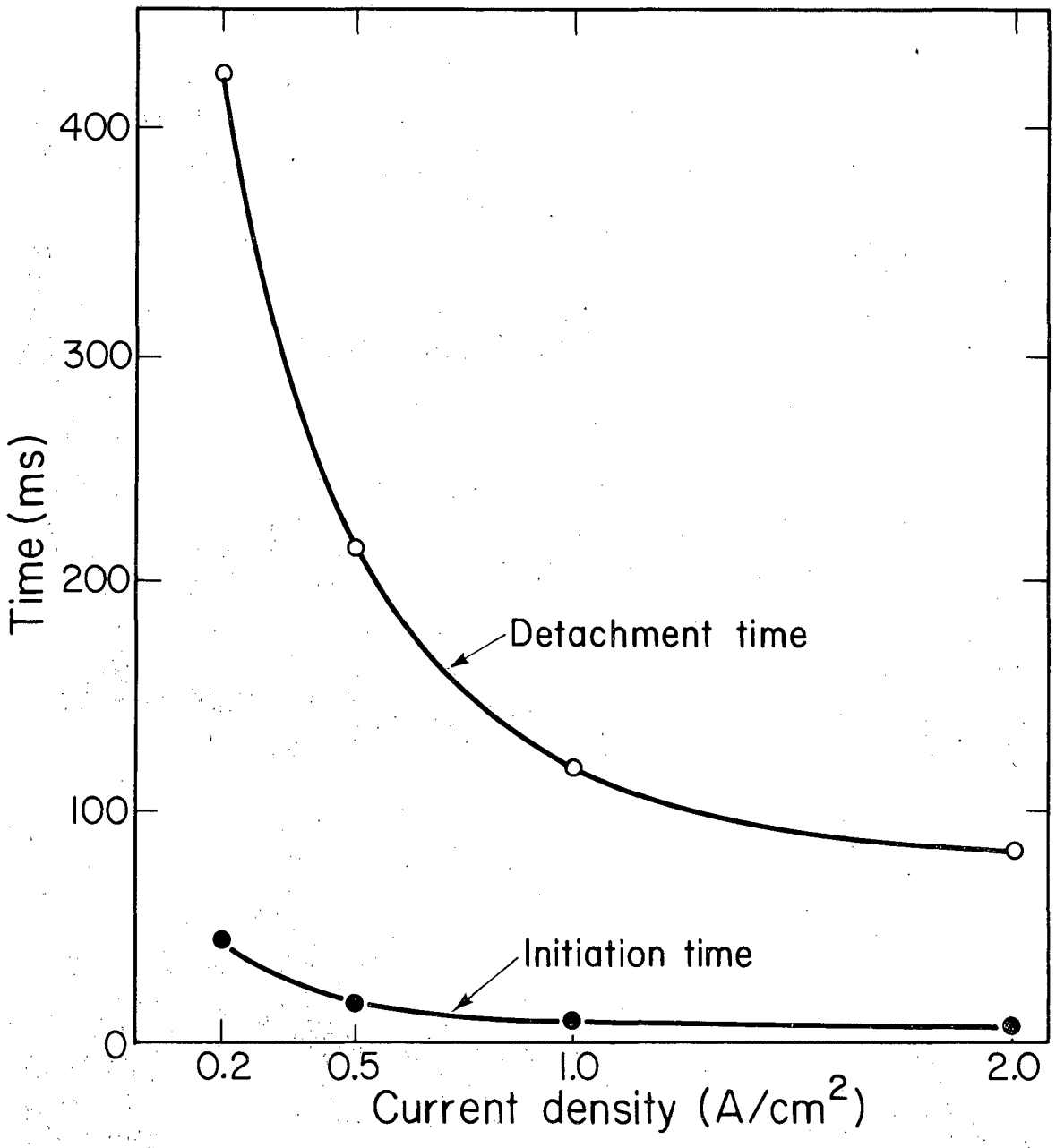
400
300
200
100
0
Time (ms)
Detachment time
Initiation time
0.2
0.5
1.0
2.0
Current density (A/cm^2)
XBL 819-1328

Fig. 3.9

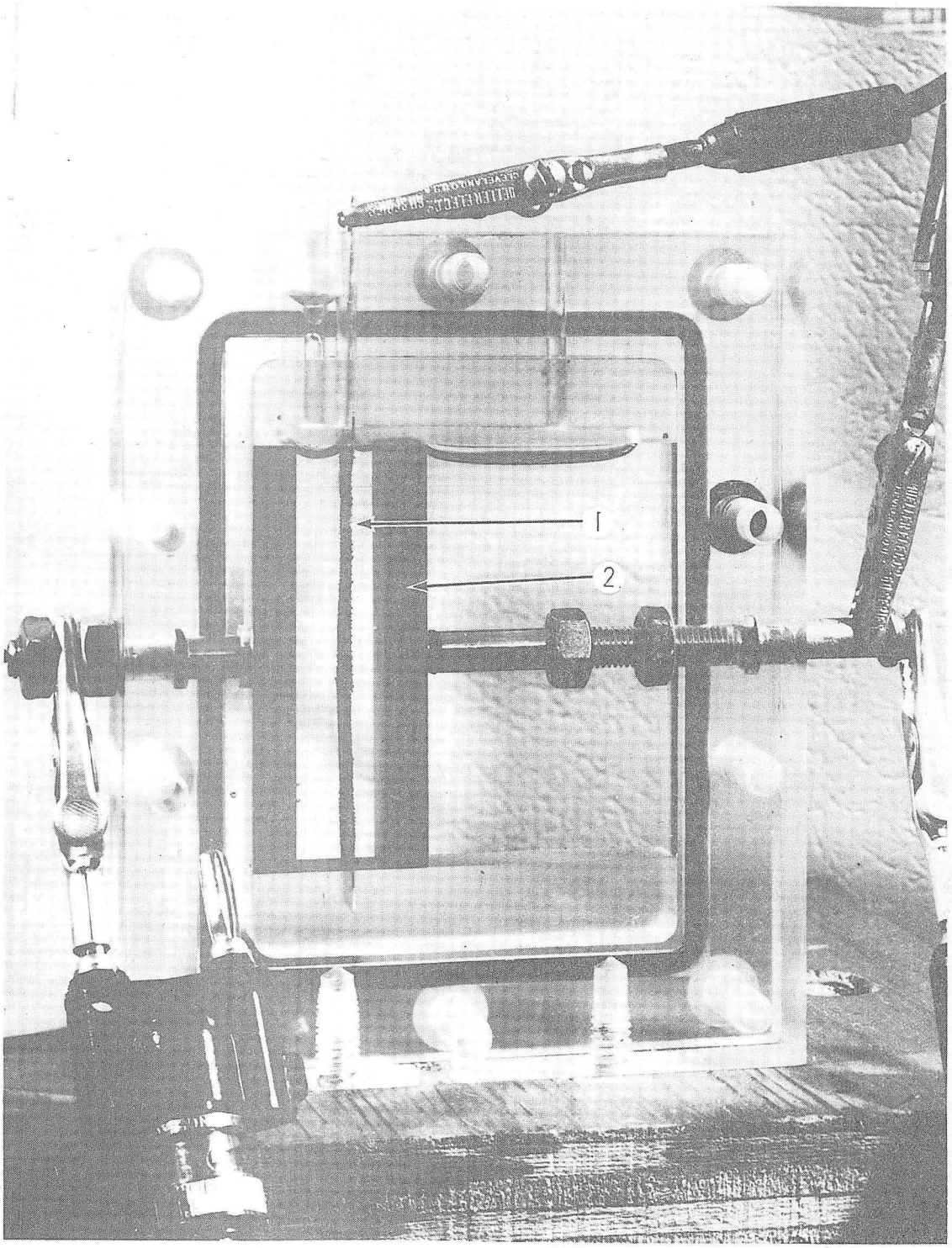

XBB 804-4912A

Fig. 4.1

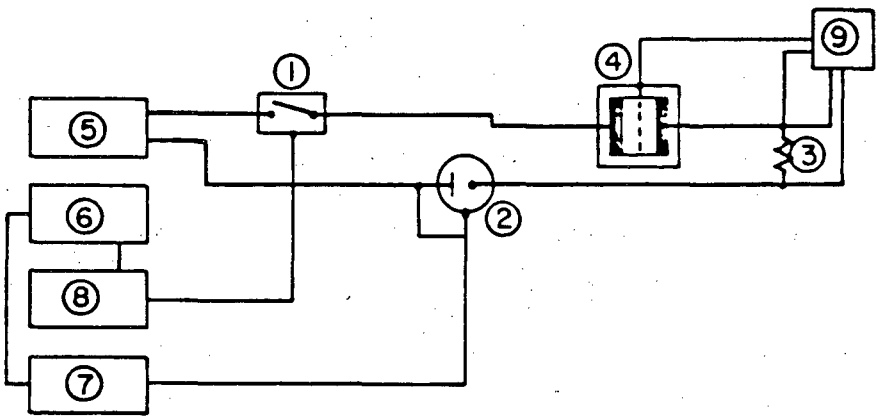

XBL 8111-1634

Fig. 4.2

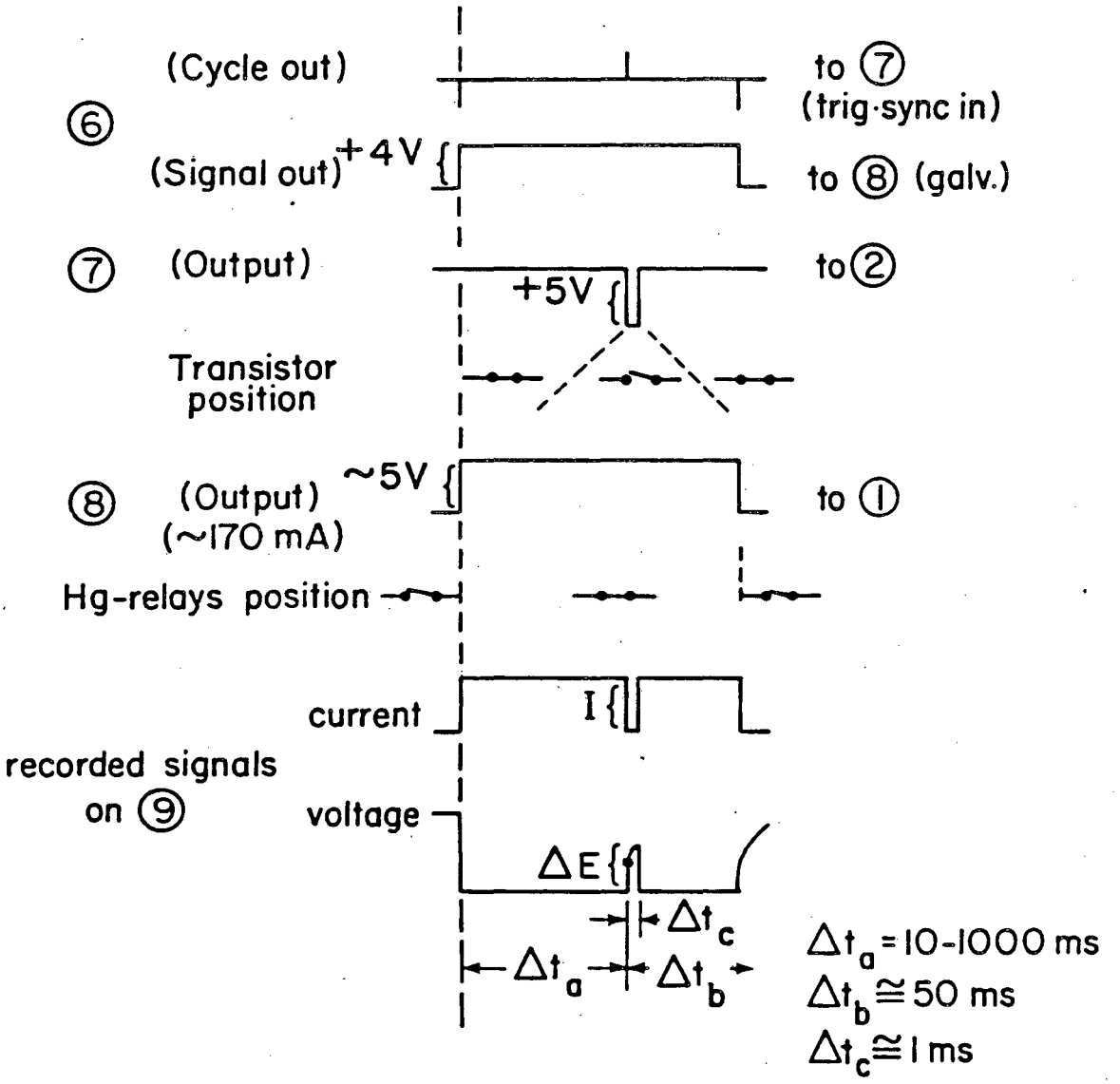
(Cycle out)
⑥
to ⑦
(trig·sync in)
(Signal out)
+4V
to ⑧ (galv.)
⑦ (Output)
to ②
+5V
Transistor position
⑧ (Output)
(~170 mA)
~5V
to ①
Hg-relays position
current
I
recorded signals on ⑨
voltage
ΔE
Δt_c
Δt_a
Δt_b
Δt_a = 10-1000 ms
Δt_b ≅ 50 ms
Δt_c ≅ 1 ms
XBL 8111-1633

Fig. 4.3

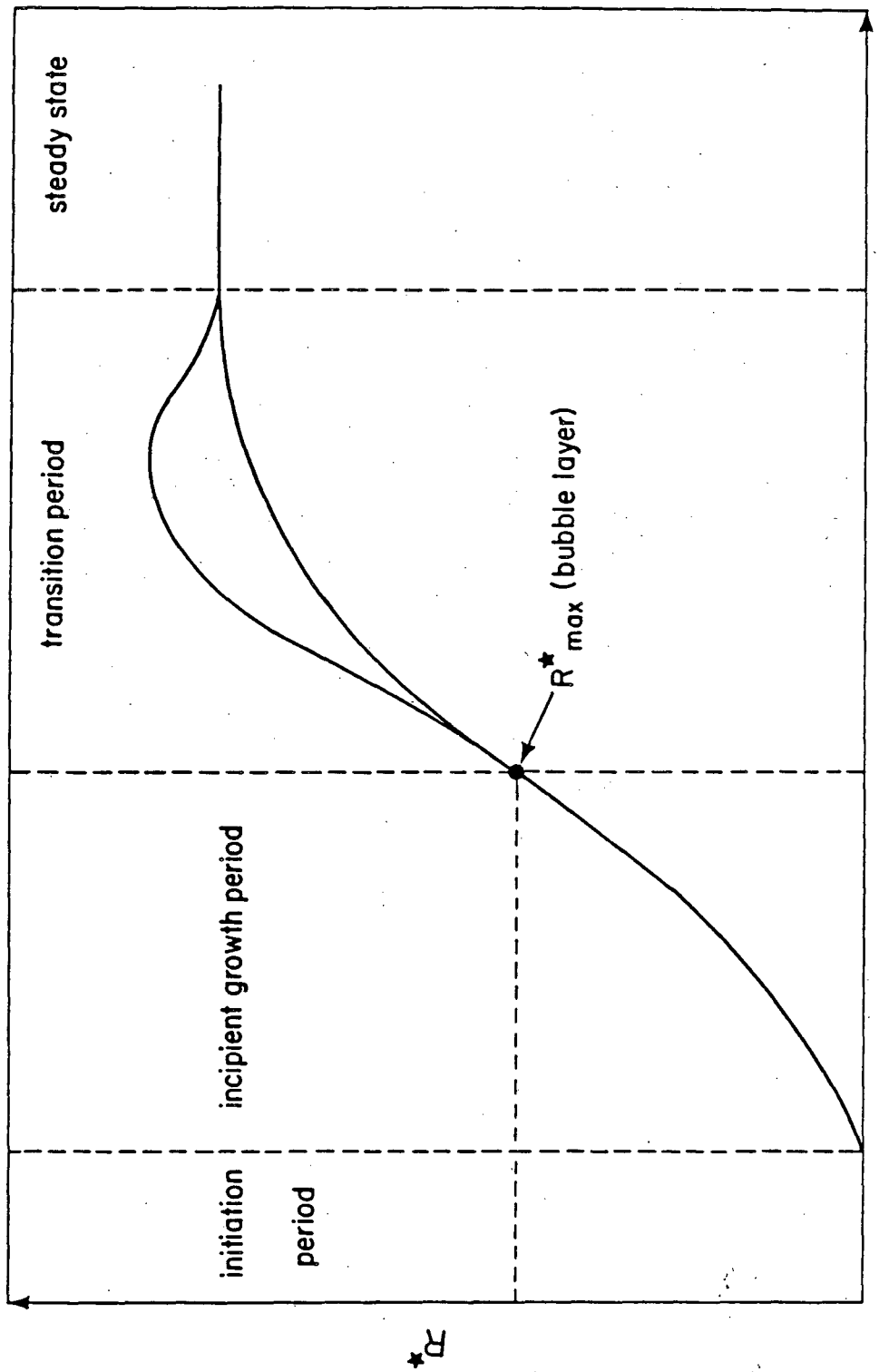

XBL 8111-1632

Fig. 4.4

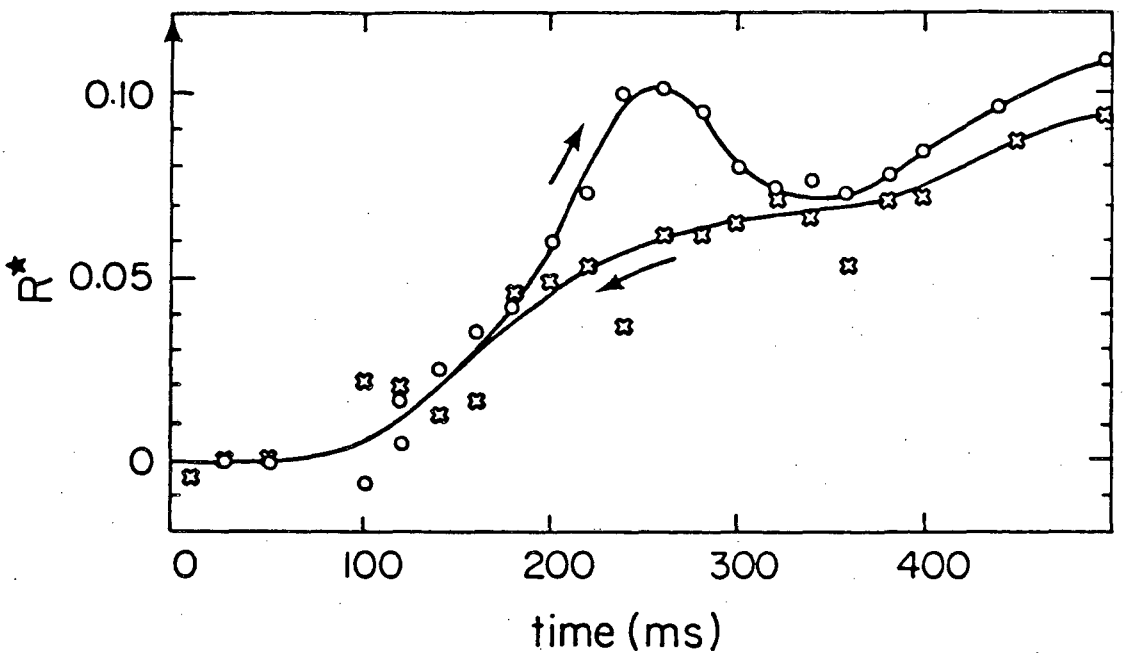

XBL 8111-1627

Fig. 4.5

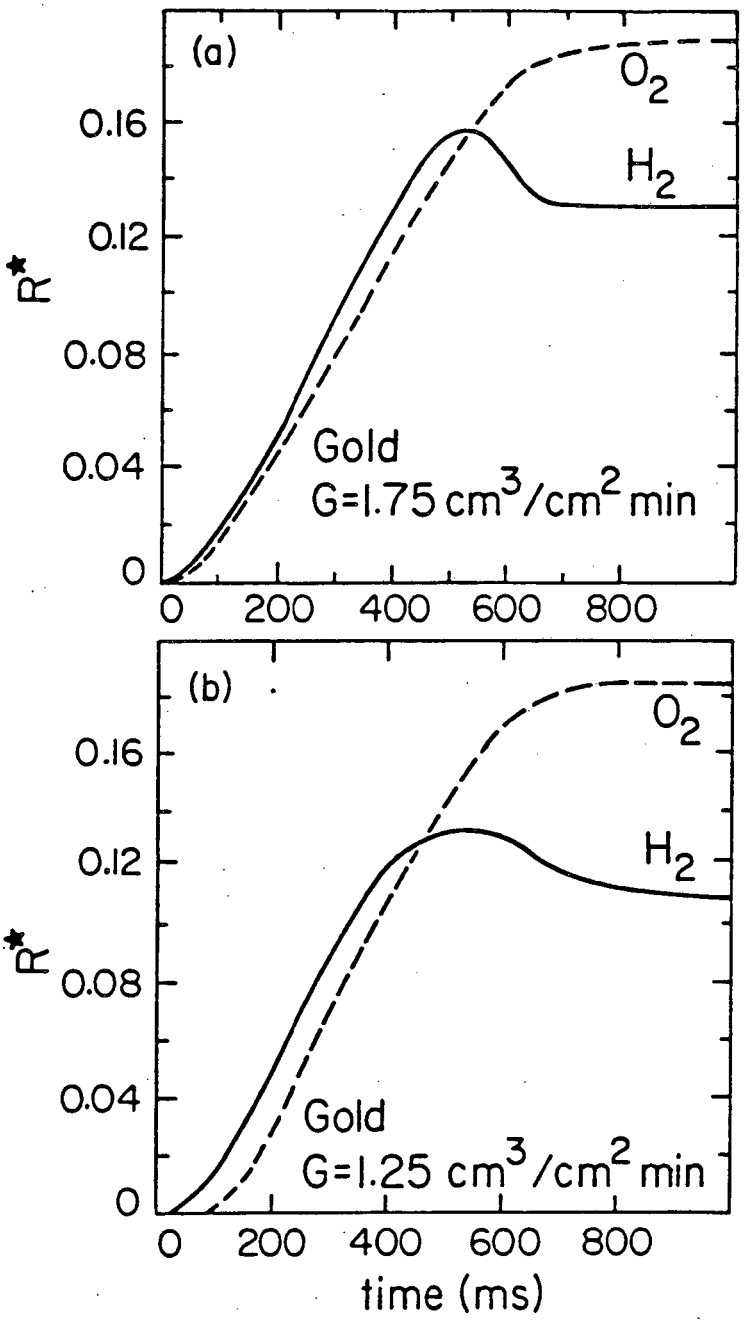

XBL 8111-1629

Fig. 4.6a-b

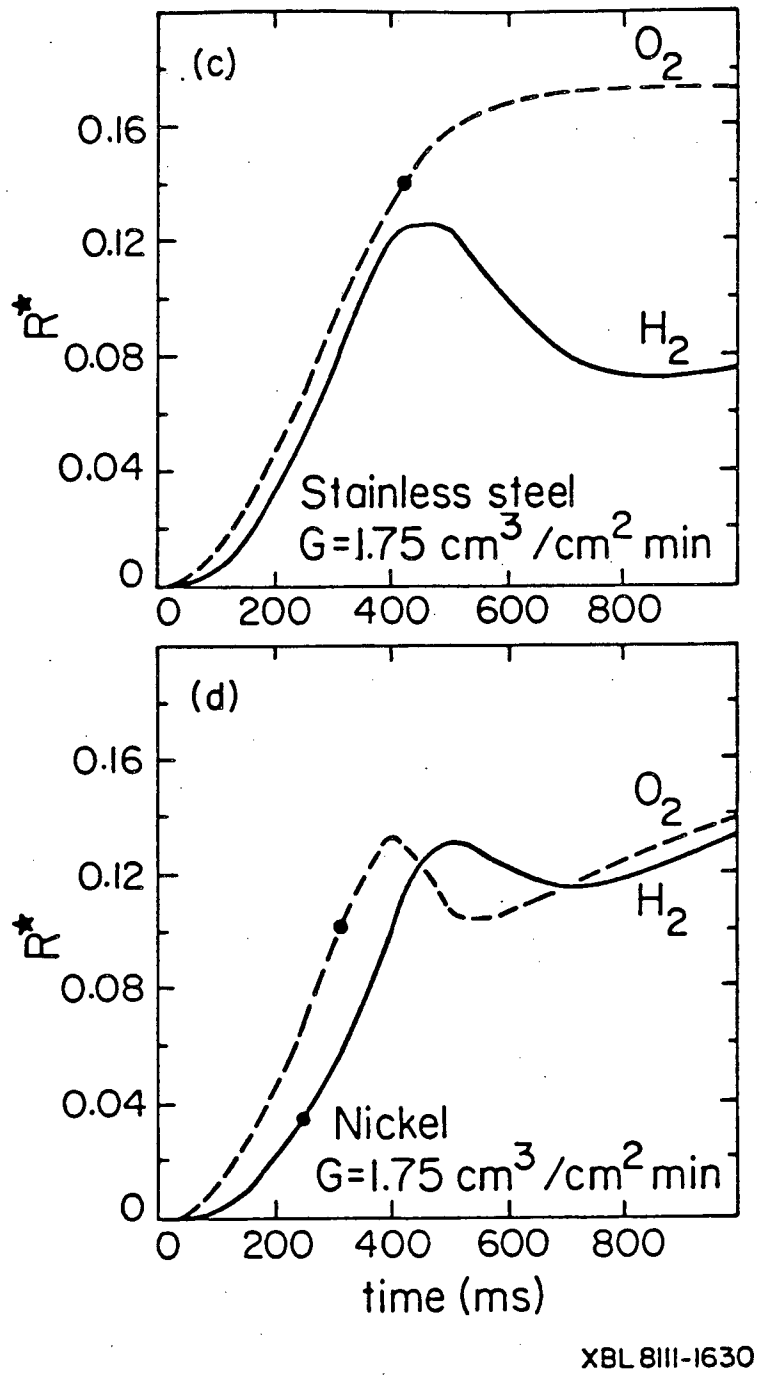
(c)
O_2
H_2
Stainless steel
G=1.75 cm^3/cm^2 min
(d)
O_2
H_2
Nickel
G=1.75 cm^3/cm^2 min
R^*
0.16
0.12
0.08
0.04
0
0
200
400
600
800
time (ms)
XBL 8111-1630

Fig. 4.6c-d

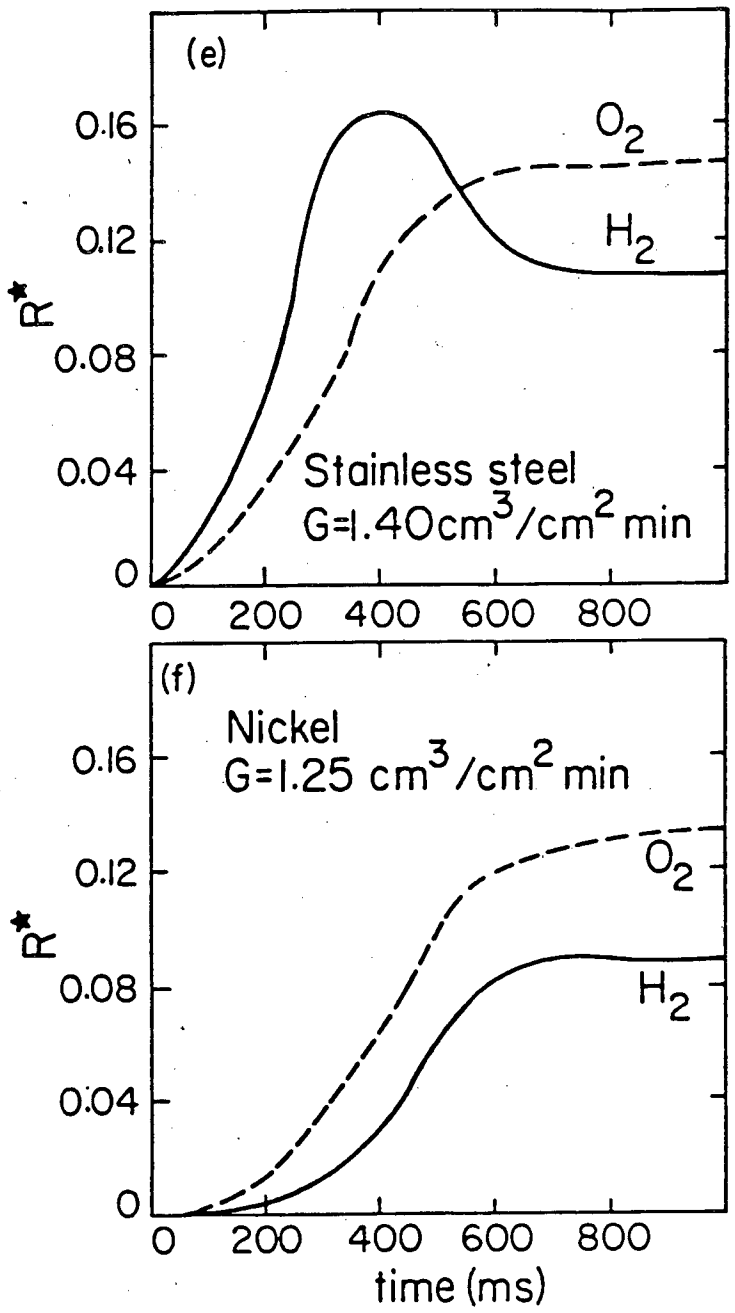

XBL 8111-1631

Fig. 4.6e-f

CONSTRICTION MODEL

$$\frac{1}{k^*} = \sqrt{\frac{1}{f(1-f)}} \tan^{-1} \sqrt{\frac{f}{1-f}}$$

DISTRIBUTION MODEL

$$k^* = \frac{8(2-\epsilon)(1-\epsilon)}{(4+\epsilon)(4-\epsilon)}$$

k^* = Conductivity ratio
f = Electrode coverage ($= n\pi d^2/4$)
ϵ = Void fraction ($= n\pi d^2/6$)

XBL 819-1327

Fig. 5.1

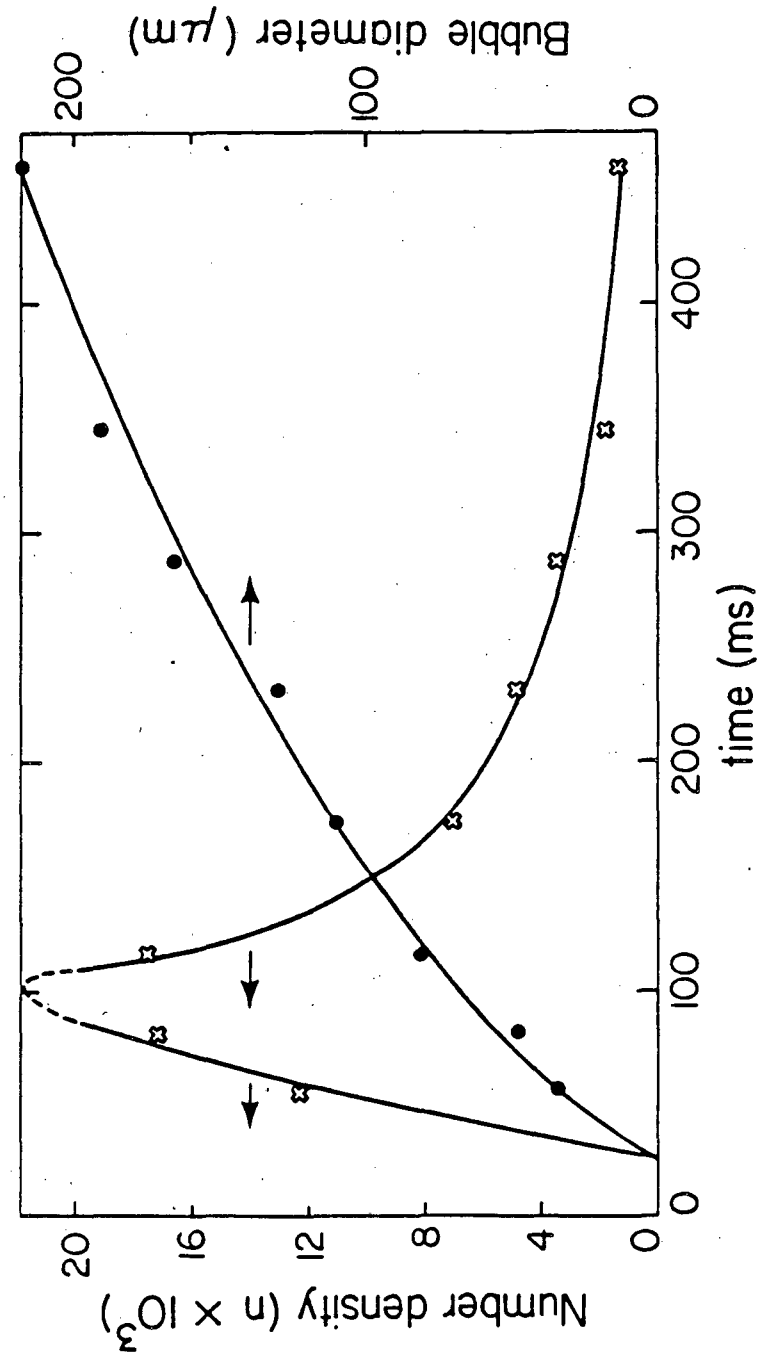

XBL 8111-1628

Fig. 5.2

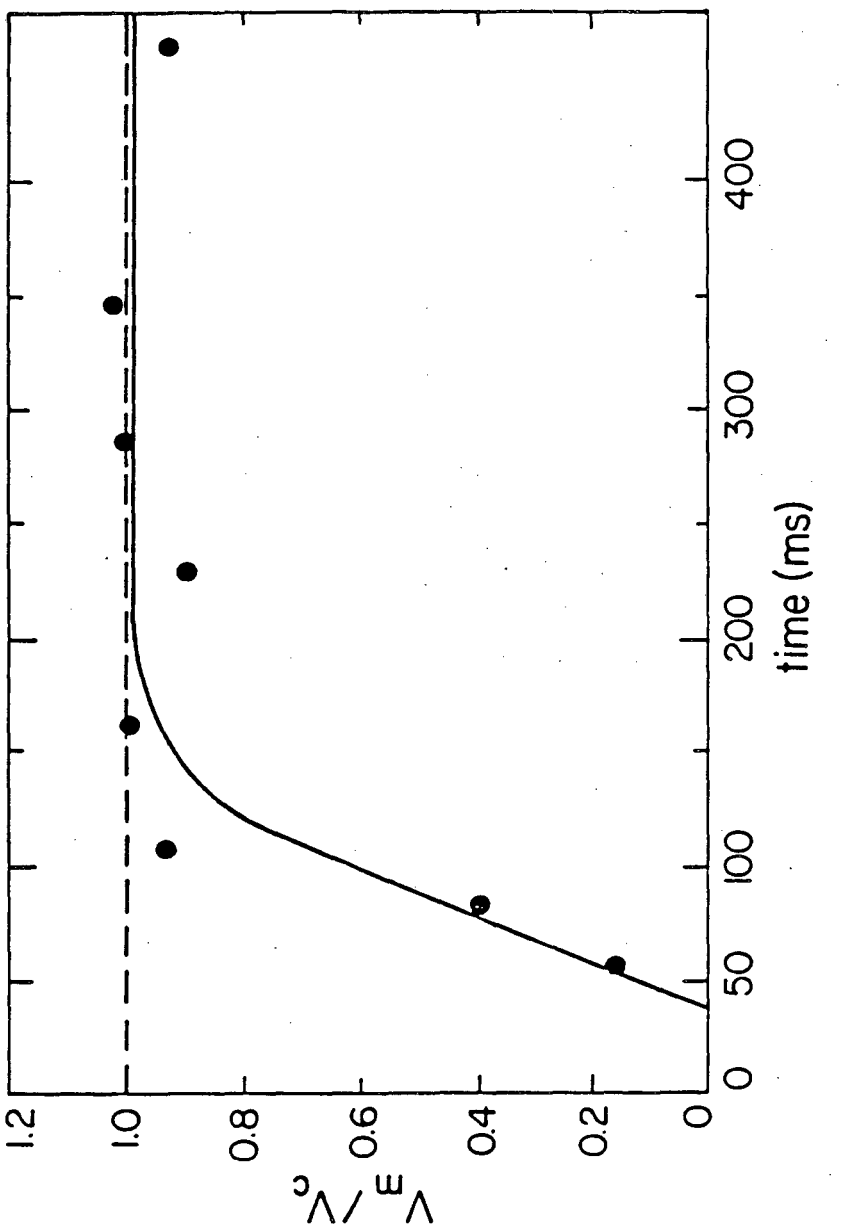

XBL 8111-1626

Fig. 5.3

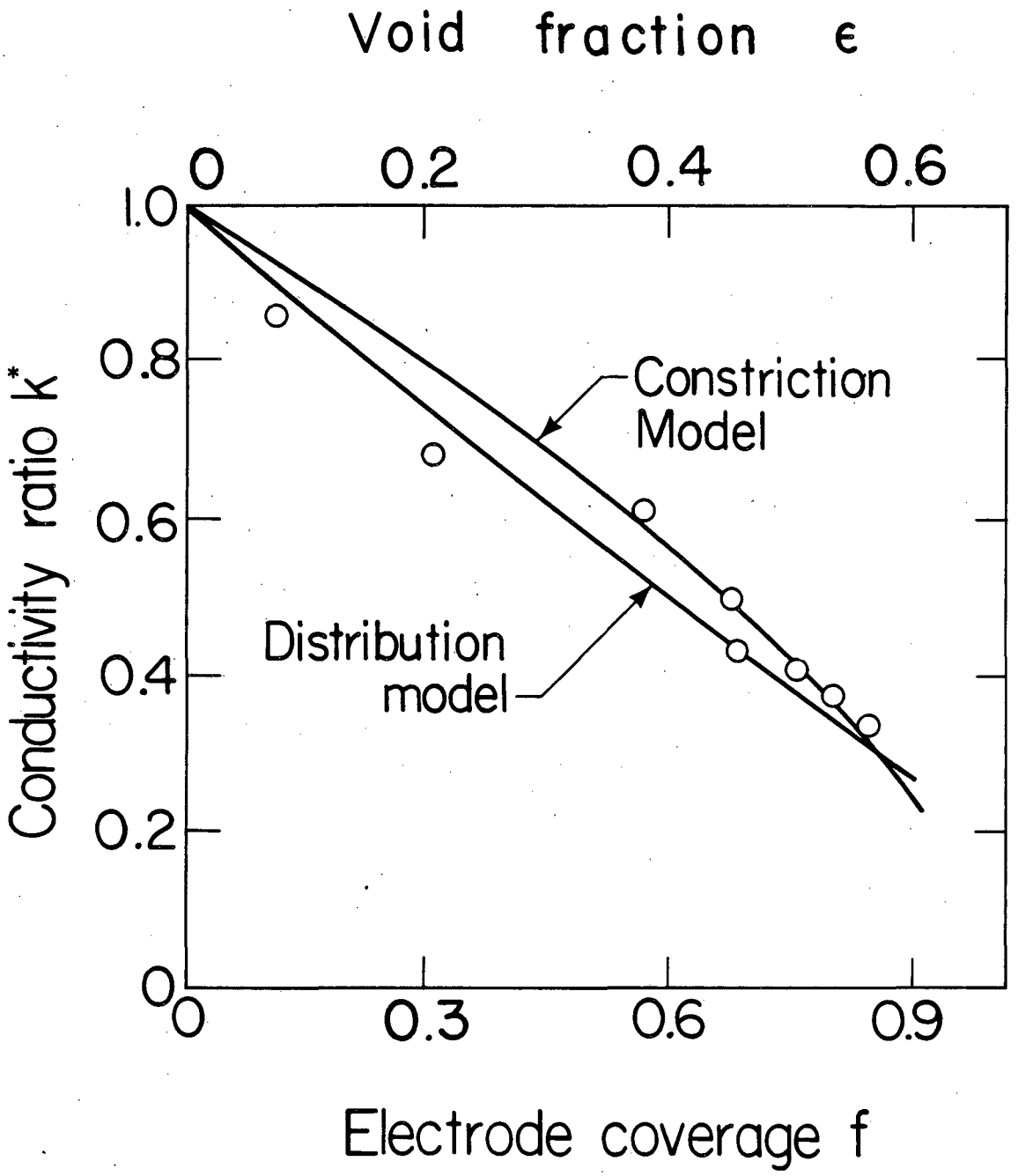

XBL 819-1310

Fig. 5.4

TECHNICAL INFORMATION DEPARTMENT
LAWRENCE BERKELEY LABORATORY
UNIVERSITY OF CALIFORNIA
BERKELEY, CALIFORNIA 94720